Noncongruence of the nuclear liquid-gas and deconfinement phase transitions

Matthias Hempel[*]
Department of Physics, University of Basel, Basel, Switzerland

Veronica Dexheimer[†]
Department of Physics, Kent State University, Kent, Ohio 44242, USA

Stefan Schramm[‡]
FIAS, Johann Wolfgang Goethe University, Frankfurt, Germany

Igor Iosilevskiy[§]
Joint Institute for High Temperature of RAS, Moscow, Russia and Moscow Institute of Physics and Technology (State University), Moscow, Russia

(Received 15 February 2013; published 23 July 2013)

First-order phase transitions (PTs) with more than one globally conserved charge, so-called noncongruent PTs, have characteristic differences compared to congruent PTs (e.g., dimensionality of phase diagrams and location and properties of critical points and end points). In the present article we investigate the noncongruence of the nuclear liquid-gas PT at subsaturation densities and the deconfinement PT at high densities and/or temperatures in Coulombless models, relevant for heavy-ion collisions and neutron stars. For the first PT, we use the FSUgold relativistic mean-field model and for the second one the relativistic chiral SU(3) model. The chiral SU(3) model is one of the few models for the deconfinement PT, which contains quarks and hadrons in arbitrary proportions (i.e., a "solution") and gives a continuous transition from pure hadronic to pure quark matter above a critical point. The study shows the universality of the applied concept of noncongruence for the two PTs with an upper critical point and illustrates the different typical scales involved. In addition, we find a principle difference between the liquid-gas and the deconfinement PTs: in contrast to the ordinary Van-der-Waals-like PT, the phase coexistence line of the deconfinement PT has a negative slope in the pressure-temperature plane. As another qualitative difference we find that the noncongruent features of the deconfinement PT become vanishingly small around the critical point.

DOI: 10.1103/PhysRevC.88.014906 PACS number(s): 05.70.Fh, 25.75.Nq, 21.65.−f, 26.60.−c

I. INTRODUCTION

Nuclear matter is expected to undergo two different major phase transitions (PTs): the liquid-gas phase transition (LGPT) of nuclear matter at subsaturation densities and moderate temperatures and the deconfinement and chiral symmetry restoration PT at high densities and/or temperatures. For convenience we will call the latter also the quark hadron phase transition (QHPT) or QCD PT. These two PTs are actively discussed in the contexts of heavy-ion collisions and astrophysics. The latter includes the interior of compact stars, i.e., neutron stars (NS) or so-called hybrid stars which have quark matter in their core.

Various effective models for nuclear matter which are constrained by properties of nuclei have shown that the LGPT of bulk uniform nucleonic matter, i.e., consisting of neutrons and protons without Coulomb interactions, is of first order (see Refs. [1,2] for two recent examples of microscopic models). Furthermore, there is also experimental evidence for this from intermediate-energy heavy-ion collisions [3–5]. On the other hand, for smaller systems the LGPT is also found to have critical behavior [6,7].

For the QHPT the situation is more uncertain. *Ab initio* solutions of QCD exist only for very high densities and/or temperatures [8–12]. Simulations on the lattice have shown that the QHPT is a smooth crossover at vanishing density. Unfortunately their use at finite densities is problematic because they suffer from the so-called sign problem. It is a numerical problem found in quantum-mechanical systems of fermions which comes from the fact that at finite chemical potential the fermion determinant is complex (see Refs. [13,14] and references therein for details). As a consequence, effective models for QCD matter have to be used, resulting in different varieties of possible QCD phase diagrams [15–32]. Many of these models predict that the QCD PT at low temperatures is of first order like the LGPT, but some also predict a crossover transition in this regime. In the present investigation we assume that both the LGPT and the QHPT are of first order and concentrate on the detailed thermodynamic aspects of the two phase transitions and especially their noncongruent features.

A noncongruent phase transition (NCPT) naturally occurs for a first-order PT with more than one globally conserved charge. In this case it becomes possible that the local concentrations of the charges vary during a phase transformation, i.e., the crossing of a phase-coexistence region. This leads to

[*]matthias.hempel@unibas.ch
[†]vdexheim@kent.edu
[‡]schramm@th.physik.uni-frankfurt.de
[§]iosilevskiy@gmail.com

qualitative differences compared to congruent PTs. Consider, for example, a phase diagram in the temperature-pressure plane. For a given temperature, a NCPT occurs over a range of pressure, related to a range of local concentrations of the charges. For a congruent PT, the equilibrium conditions can be fulfilled only at a single value of the pressure for each temperature. As we will show, also other characteristics of PTs depend on the number of globally conserved charges. It is the main scope of the present article to identify and discuss these noncongruent features.

As will be explained below, isospin symmetric matter is an "azeotrope," which means that it leads to a congruent PT even though it consists of more than one globally conserved charge. Consequently, the noncongruent features only become visible for an isospin asymmetric system and are, thus, highly related to the isospin asymmetry. Phase diagrams of isospin asymmetric matter are of extreme importance for the complete understanding of QCD and nuclear matter. They are highly related to the symmetry energy, as explained, e.g., in Refs. [33–35]. Such studies are also used to analyze the effect of model parameters on the QCD phase diagram [36–39]. The effect of different isospin/charge assumptions has been studied already extensively in the literature for the LGPT [35,40–45], and also experimentally [46,47], and for the QHPT [36,38,48] as well. Some authors [43,45,48–50] have stated that the LGPT and QHPT changes from first to second order (according to the Ehrenfest classification) if one goes to an asymmetric system. This was concluded from the nonstandard behavior of thermodynamic quantities during an isothermal crossing of the two-phase region. One of the main statements of the present paper is that this nonstandard behavior in asymmetric matter is the typical manifestation of a noncongruent first-order PT.

In the present article, the LGPT and the QHPT are studied for the scenarios of heavy-ion collisions of symmetric and asymmetric nuclei. For the QHPT, we are also investigating the scenario of the interior of a neutron (respectively, hybrid star). For this purpose we use a relativistic chiral SU(3) effective model. This model predicts that both the LG and the QCD PT at low temperatures are of first order. Due to technical reasons, the chiral SU(3) model is applied only for the QHPT. For the description of the LGPT we apply the FSUgold relativistic mean-field model. Even using only one selected theoretical model for the QHPT and one for the LGPT, our main conclusions are to some extent model independent, because the applied thermodynamic concepts are rather universal.

The structure of this article is as follows: in Sec. II we discuss various aspects of (non-)congruence of PTs in detail. In Sec. III we describe the effective model used for the calculations of the LGPT, the FSUgold equation of state (EOS). In Sec. IV we continue with the description of the chiral SU(3) model for the QHPT. In Sec. V we specify our thermodynamic model and setup used for the two PTs and the different physical systems. In Sec. VI we analyze and compare in detail the results for the different scenarios, with a focus on the structure of the resulting phase diagrams and the noncongruent features. In Sec. VII we summarize our main findings and draw conclusions.

II. CONGRUENCE/NONCONGRUENCE OF PHASE TRANSITIONS

A. Definition of noncongruence

The term "noncongruent" (or "incongruent") phase transition (NCPT) denotes the situation of phase coexistence of two (or more) macroscopic phases with different chemical compositions (see the IUPAC definition [51] and Ref. [52]). Such systems are also called "binary," "ternary," etc., in contrast to "unary" systems. NCPTs have been well known for many years in many terrestrial applications as a particular type of PT (regardless of the term), e.g., in low-temperature solution theory (see, e.g., Ref. [53]), in the theory of simple liquid mixtures of hydrocarbons (see, e.g., Ref. [54]), or in the theory of crystal-fluid and crystal-crystal phase diagrams in chemical compounds. NCPTs also have been known in nuclear physics [42], in heavy-ion physics [55], and also in the physics of compact stars [56] for quite some time, but the term "noncongruent" has been introduced to these areas of physics only recently (see below).

The variants of terrestrial NCPT which are the closest to LGPTs and QHPTs discussed in the present article are PTs in high-temperature, chemically reacting, and partially ionized plasmas—typical products of extremely heated chemical compounds. NCPTs were studied thoroughly for high-temperature uranium-oxygen systems during hypothetical "severe accidents" in the framework of nuclear reactor safety problems [57–62]. The universal nature of this type of PT and its applicability for most astrophysical objects was claimed and illustrated in Ref. [62], using the examples of (hypothetical) plasma PTs in the interiors of Jupiter and Saturn, brown dwarfs, and extrasolar planets. The identification that most PTs in neutron stars are noncongruent, in particular for the QHPT in hybrid stars, was presented at several conferences by I.I.[1] and then published recently in Ref. [52]. By now, the term "noncongruent" PT is already used in the astrophysical literature [49,63]. Our theoretical description of the LGPT and QHPT as noncongruent phase transitions in the present study is based essentially on experience from terrestrial applications.

It should be noted that in the above standard terrestrial definition of NCPTs, different ionized states of atoms or molecules are not relevant for the possible noncongruence but only the number of chemical elements. The additional degree of freedom of ionization does not count in the definition because one deals with phase coexistence of two electroneutral macroscopic phases (or a mixture of several electroneutral macroscopic fragments). For macroscopic phases, Coulomb interactions automatically lead to local charge neutrality and thereby suppress this degree of freedom. Conversely, for all thermodynamic systems in the present paper, including those corresponding to matter in neutron stars, Coulomb interactions are not taken into account explicitly, in spite of the presence of charged species (protons, quarks, leptons, etc.). This is what we call a "Coulombless" model description. In such a Coulombless approach, positive and

[1] See, e.g., http://www.triam.kyushu-u.ac.jp/ICPP/program/download/11-I-w03.pdf

negative charges (e.g., nuclei and electrons) play the role of different chemical elements. In nuclear matter the abundance of chemical elements is typically not conserved but only some generalized "charges," like baryon number, electric charge, and possibly also isospin or strangeness. The generalization of the definition of noncongruence to first-order PTs in dense nuclear matter, described as Coulombless systems with more than one conserved charge, is, thus, obvious: phase coexistence of two (or more) macroscopic phases with different composition of the charges, including electric charge.

There is a famous example from the context of neutron stars which illustrates the definition of noncongruence: in β-equilibrated, cold neutron stars baryon number and total net electric charge (which has to be zero) are two conserved charges. There are two typical choices for the treatment of charge neutrality for PTs of macroscopic phases within the Coulombless approximation. In the first case, one assumes local charge neutrality, with zero net charge in both phases, and, thus, one obtains a congruent PT of a unary system. Because here the congruence is enforced by the requirement of local charge neutrality, we call it, more specifically, a "forced-congruent" PT, as proposed in Ref. [52]. In astrophysics, this scenario is usually called the "Maxwell-PT," which is then used as a synonym for congruent phase transitions in general. In the second case one assumes global charge neutrality. In this case the two coexisting phases will have electric charge concentrations of opposite sign. Consequently, the system is binary and the PT is noncongruent [56]. In astrophysics this is often called the "Gibbs-PT" and again taken as a synonym for noncongruent PTs in general. The classification with respect to "Gibbs" or "Maxwell" of matter in supernovae or protoneutron stars with possibly trapped neutrinos was given in Ref. [64]. Nuclear matter in heavy-ion collisions also has more than one conserved charge, namely net baryon number, net electric charge, and also net weak flavor (respectively, isospin), due to the fast time scales involved. Thus, Coulombless PTs in heavy-ion collisions will in general also be noncongruent, see also Ref. [55]. The authors of Ref. [65] address experimental consequences of the QHPT as a noncongruent PT. The previous arguments are valid for both PTs, LGPT and QHPT, just the typical scales involved and the quantitative behavior differ.

B. Coulomb interactions

As mentioned before, it should be stressed that for all thermodynamic systems in the present paper we are using a "Coulombless" model description. Also, surface effects are neglected in our work. As a consequence, the two-phase mixtures at equilibrium (i.e., not metastable) within the two-phase regions are always described as coexistence of two *macroscopic* phases.

The simplification of Coulombless is to some extent reasonable for the theoretical description of relativistic heavy-ion collisions, where one has a net electric charge but Coulomb energies are small compared to the typical collision energies. Furthermore, the long-range nature of Coulomb forces could be ignored in view of the small size of the ensemble of heavy-ion collisions products. However, for the same reason, it is questionable whether the thermodynamic limit is fulfilled [66]. On the other hand, for the description of nuclear clusters appearing in the nuclear liquid-gas PT of low-energy heavy-ion collsions, Coulomb and surface energies are in fact crucial. Nevertheless, the bulk Coulombless treatment gives useful insight into the main characteristics of the PT.

Matter in neutron stars has to be overall charge neutral in order to be gravitationally bound. In this case, Coulomb interactions and corresponding surface effects can be included in a more detailed mesoscopic description, leading to structured mixed phases. Usually these phases with finite-size substructures are called the "pasta phases" [67–72] or "pasta plasma" [52]. The classification with respect to noncongruence of these scenarios is somewhat still an open question [52]. In a strict thermodynamic sense, the state of matter in such mesoscopic calculations should not be seen as the two-phase coexistence of a first-order PT but rather as a sequence of single phases with nonuniform substructure.

A very low surface tension between the two phases (see Refs. [32,73] for possible calculations of the surface tension) would lead to a highly dispersed charged and nonsoluble mixture of microfragments of one phase into the other, a mixed phase, which also could be called a charged "emulsion."[2] We note that very often in the astrophysical literature, matter in the two-phase coexistence region of any PT, including those in neutral systems, is generally said to be in a "mixed phase." We think it is more accurate to denote this as a "two-phase mixture" and to reserve the term "mixed phase" only for the state of matter obtained in the mesoscopic description of PTs in Coulomb systems with a low surface tension, as described above.

Without a detailed mesoscopic treatment, the effect of Coulomb interactions in NSs can be estimated by different assumptions for charge neutrality [74–77], which we will use in the present study. The assumption of local charge neutrality, used in the "Maxwell-PT," which was already introduced above, corresponds to the limit of an infinitely high surface tension between the two phases. In terrestrial plasmas, phase equilibrium of locally charge neutral phases with Coulomb forces is denoted more accurately as the Gibbs-Guggenheim conditions for phase equilibrium, see, e.g., Ref. [52]. Conversely, the usage of global charge neutrality (GCN) for macroscopic phases in a Coulombless approach can be seen as an approximation for the case of a vanishing surface tension in the mesoscopic description. In astrophysics, this is typically called the "Gibbs-PT" [56].

C. Characteristics of noncongruent PT

It was shown in Refs. [42,43,52,55–62] and many others, and it will also be shown below, that noncongruency significantly changes the properties of all PTs, namely (a) there is a significant impact on the phase transformation dynamics, i.e., a strong dependence of the PT parameters on the rapidity of the transition [60]. (b) The thermodynamics of

[2]Another term (a culinary one, like "pasta," "spaghetti," etc.) was proposed for this emulsion-like mixture: "milk phase" i.e., a highly dispersed mixture of oil microdrops in water [52].

PTs becomes more complicated. The essential changes include (i) a significant change in the properties of the singular points (critical point in particular) and a separation of the critical point and end points, such as the temperature end point, pressure end point, etc., and (ii) a significant change in the scale of two-phase boundaries in extensive thermodynamic variables (say P-V, V-T, H-T, etc.) and even in the topology of all two-phase boundaries in the space of all intensive thermodynamic variables, i.e., pressure, temperature, specific Gibbs free energy, and so on. Note that this is valid for both types of PTs: with and without a critical point (e.g., gas-liquid-like PT and crystal-fluid-like PT, correspondingly). One of the most remarkable consequences of the noncongruence in the NCPT is the appearance of a two-dimensional "banana-like" region instead of the well-known one-dimensional P-T saturation curve for ordinary (congruent) PTs (see Fig. 1 in Ref. [52]). The same should be expected in the plane of the widely used pair of variables: temperature-baryon chemical potential (see below). (iii) Closely connected to this is the significant change of the behavior in the two-phase region: i.e., isothermal and isobaric crossings of the two-phase region no longer coincide. The isothermal NCPT starts and finishes at different pressures, while the isobaric NCPT starts and finishes at different temperatures. Basically, the pressure on an isotherm monotonically increases with density.

Aspect (iii) of NCPTs is well studied in the context of neutron stars [56]. Inside a neutron star, the pressure has to decrease monotonically with the radius. A congruent PT leads, therefore, to a spatial separation of the two coexisting phases, with a discontinuous jump in density and all extensive thermodynamic variables at the transition radius inside the neutron star. Conversely, for a NCPT, a spatially extended two-phase coexistence region is present, with a continuous change of total density, total energy density, etc., throughout. We remark that for the LGPT there exist several works which also have discussed the other characteristic features of NCPTs and only used a partially different terminology, see, e.g., Refs. [42,43,45]. For the QHPT, the possible noncongruence has not been discussed in such detail as is done here.

Furthermore, there are still publications that do not treat the thermodynamic aspects of nonunary phase transitions, i.e., the noncongruent features, in a proper way. For example, aspect (iii) sometimes led to the conclusion that one has a second-order PT according to the Ehrenfest classification, as, e.g., in Refs. [43,45,48–50]. However, the two coexisting phases have different order parameters, like densities, entropies, asymmetries, etc., and, most importantly for our purposes, different generalized "chemical" compositions. At the interface between the two macroscopic phases there is a discontinuous jump of the order parameter and, thus, the PT is still of first order. Moreover, the first two aspects of (b) from above are sometimes overseen or neglected in the literature, which means that the noncongruence is not fully taken into account (compare, e.g., with Ref. [1]).

D. Isospin symmetry, azeotrope

The isospin symmetry of strong forces plays an important role for the possible noncongruence of the LGPT and the QHPT. Independently of density and temperature, isospin symmetric nuclear matter always represents the state with the lowest thermodynamic potential (neglecting Coulomb interactions and assuming equal masses of protons and neutrons). Thus, the isospin chemical potential is zero for symmetric nuclear matter. As a consequence, isospin does not appear as a relevant charge for symmetric nuclear matter because this degree of freedom is not explored, i.e., even in a first-order PT the involved phases remain symmetric. Therefore, the LG and QH PTs remain congruent if the system is exactly symmetric and if no other globally conserved charge than baryon number is involved (see also Appendix B). This is called "azeotropic" behavior, denoted for a system with more than one conserved charge whose charge ratios cannot be changed by distillation for a certain azeotropic composition. The ensemble of such azeotropic points in the parameter space, e.g., for all temperatures, is called an azeotropic curve. Note that the isospin asymmetry of the hot state of matter in a heavy-ion collision experiment is mainly set by the initial charge-to-mass ratio Z/A of the colliding nuclei, e.g., $Z/A \simeq 0.4$ in Au + Au collisions.

E. Unified equation of state

As mentioned in point (i) in Sec. II C, another consequence of noncongruent phase transitions is the possible emergence of critical points, which differ from the points of maximum temperature, pressure, or extremal chemical potential. To obtain such critical points and end points at all, it is necessary that both of the two involved phases are calculated with the same theoretical model ("unified" or "single" EOS approach). In other words, one has to use only one underlying many-body Hamilton operator. This is in contrast to a "two-EOS" approach, where two different EOS models are applied for the two phases in coexistence. Such a "two-EOS" description can have several shortcomings, as it cannot contain critical points and end points (see Appendix A and the standard literature, e.g., Ref. [53]) and it does not give a consistent description of metastable or unstable matter in the binodal (respectively, spinodal regions), e.g., for a liquid-gas type PT. In summary, in the "unified" EOS approach both coexisting phases are presumed as isostructural (like gas and liquid) with a possible continuous transition from one phase into another, while in the two-EOS approach this is impossible.

Almost all studies of the LGPT are based on the unified EOS approach. This also applies for our investigation of the LGPT with the FSUgold relativistic mean-field model. Unified EOS approaches for the QHPT are usually built with either only hadrons or only quarks. Thus, they do not give the expected degrees of freedoms for one of the two phases. Alternatively, often the two-EOS approach is applied for the QHPT (see, e.g., Ref. [48]) to have the right degrees of freedom. On the other hand, this approach cannot contain all possible noncongruent features of the singular points, as explained above. The chiral SU(3) model used in the present study is one of the few unified-EOS approaches for the QHPT that contains hadronic as well as quark degrees of freedom. These can appear, in principle, in arbitrary proportions (solution-like

mixture[3]) with the interactions leading to the correct behavior for low (respectively high) densities and temperatures. See Refs. [23,78] for another unified-EOS model that also contains hadronic and quark degrees of freedom. Another exception of a unified-EOS approach for the QHPT with the correct degrees of freedom is the EOS of Ref. [79], where the two-EOS approach is transformed into a one-EOS version with the use of a special spline-based interpolation procedure.

III. FSUGOLD RMF MODEL

For the LGPT of nucleonic matter we apply a relativistic mean-field (RMF) model. In principle, the chiral model also could be used for this, as it also contains the LGPT [80]. However, due to the different characteristic scales involved and for numerical reasons, we use a dedicated model for the LGPT which occurs at subsaturation densities. We choose the FSUgold RMF parametrization [81] because of its excellent description of matter around and below saturation density and because its neutron matter EOS is in agreement with recent experimental and observational constraints (see, e.g., Ref. [82]). Its Lagrangian is based on the exchange of the isoscalar-scalar σ, the isoscalar-vector ω, and the isovector-vector ρ mesons between nucleons. Particularly for FSUgold, the coupling between the ω and the ρ meson is also included. This leads to a better description of nuclear collective modes, the EOS of asymmetric nuclear matter, and a different density dependence of the symmetry energy [83]. The free parameters of the Lagrangian, the meson masses and their coupling constants, are determined by fits to experimental data, more specifically to binding energies and charge radii of a selection of magic nuclei.

The only baryonic degrees of freedom in FSUgold are neutrons and protons. For the typical densities and temperatures of the LGPT, hyperonic or quark degrees of freedom are not relevant. Because FSUgold considers only the "elementary" particles of the LGPT but not any compound objects (respectively, bound complexes like light or heavy nuclei), it belongs to the class of so-called physical descriptions of PTs. In this description, all effects of bound complexes are presumed to be taken into account by the interactions ("nonideality") of the "elementary" particles (see, e.g., Ref. [84]). However, for a more detailed description of the nuclear EOS like, e.g., used in simulations of core-collapse supernovae, the formation of nuclei and nuclear clusters has to be incorporated explicitly, see, e.g., Refs. [71,85–91]. For high temperatures, light nuclei like the deuteron or α particle are most important, whereas at low temperatures, heavy and also superheavy nuclei give the dominant contribution. If all possible compound objects (i.e., nuclei) were included as a chemical mixture, one would obtain a quasichemical representation, as, e.g., done in Ref. [88]. This can cause substantial changes and even to a quenching of the liquid-gas phase transition as a first-order PT, see also Ref. [92]. However, even in this case one can use the analogy between the characteristic changes of the nuclear composition and the behavior of the gas and the liquid phases in a pure thermodynamic treatment, see, e.g., Refs. [87,93]. It has been confirmed in many studies that the mean-field without clusterization overestimates the region of instability, see, e.g., Refs. [86,94]. Because Coulomb interactions and clusterization are more important in the cold catalyzed matter of neutron stars than in the hot plasma of heavy-ion collisions, we discuss the LGPT only in the latter scenario.

[3]Another term was proposed for this solution-like mixture: "vodka phase," i.e., a solution of spirit in water with arbitrary proportion [52].

IV. CHIRAL SU(3) MODEL

The nonlinear realization of the σ model [95,96] is built on the original linear σ model [97,98], including the pseudoscalar mesons as the angular parameters for the chiral transformation, to be in better agreement with nuclear physics results. It is an effective quantum relativistic model that describes hadrons interacting via meson exchange, similarly to the FSUgold RMF interactions. However, the model is constructed in a chirally invariant manner as the particle masses originate from interactions with the medium and, therefore, go to zero at high densities/temperatures.

The Lagrangian density of the model in the mean-field approximation (all particles contribute to the global mean-field interactions and are in turn affected by them), constrained further by astrophysical data, can be found in Refs. [99–101]. In this work, we are going to use an extension of this model called the chiral SU(3) model, that also includes quarks [80]. The Lagrangian density in mean-field approximation reads as follows:

$$\mathcal{L} = \mathcal{L}_{\rm Kin} + \mathcal{L}_{\rm Int} + \mathcal{L}_{\rm Self} + \mathcal{L}_{\rm SB} - U, \tag{1}$$

where, besides the kinetic energy term $\mathcal{L}_{\rm Kin}$, the terms

$$\mathcal{L}_{\rm Int} = -\sum_i \bar{\psi}_i [\gamma_0 (g_{i\omega}\omega + g_{i\phi}\phi + g_{i\rho}\tau_3\rho) + M_i^*]\psi_i, \tag{2}$$

$$\mathcal{L}_{\rm SB} = m_\pi^2 f_\pi \sigma + \left(\sqrt{2} m_k^2 f_k - \frac{1}{\sqrt{2}} m_\pi^2 f_\pi\right)\zeta, \tag{3}$$

represent the interactions between baryons (and quarks) and vector and scalar mesons and an explicit chiral symmetry breaking term, responsible for producing the masses of the pseudoscalar mesons. $\mathcal{L}_{\rm Self}$ contains the self-interactions of scalar and vector mesons, where we refer to Refs. [80,99] for details.

Up, down, and strange quarks and the whole baryon octet are always considered in the above sum over i, in the entire phase diagram. However, the degrees of freedom which are actually populated change from hadrons to quarks and vice versa through the introduction of an extra field Φ in the effective masses of the baryons and quarks. The scalar field Φ is named in analogy to the Polyakov loop [102] since it also works as the order parameter for deconfinement. The potential for Φ reads as follows:

$$U = \left(a_0 T^4 + a_1 \mu_B^4 + a_2 T^2 \mu_B^2\right)\Phi^2 + a_3 T_0^4 \ln(1 - 6\Phi^2 + 8\Phi^3 - 3\Phi^4). \tag{4}$$

It was modified from its original form in the PNJL model [103,104] in order to also be used to study low-temperature and high-density environments (besides high-temperature and low-density environments). It is a simple form to extend

the original potential to be able to reproduce the physics of the whole phase diagram. Because U now also depends on the baryon chemical potential μ_B, it will provide an extra contribution to the total baryon density. It was shown in Refs. [24,25,105] that our choice for the potential $U(\Phi)$ can also be used in the PNJL model, successfully reproducing QCD features. Note that our finite-temperature calculations include the heat bath of hadronic and quark quasiparticles and their antiparticles within the grand canonical potential of the system. Free pions and kaons are included originally in the model but neglected here for simplicity. Further comments about their role in the scenarios which we consider are given below in Sec. V B.

With the Lagrangian above, the particle masses are generated by the scalar mesons whose mean-field values correspond to the isoscalar-scalar (σ) and isovector-scalar (δ) light quark-antiquark condensates as well as the strange quark-antiquark condensate (ζ). In addition, there is a small explicit mass term M_0 and the term containing Φ,

$$M_B^* = g_{B\sigma}\sigma + g_{B\delta}\tau_3\delta + g_{B\zeta}\zeta + M_{0_B} + g_{B\Phi}\Phi^2, \quad (5)$$

$$M_q^* = g_{q\sigma}\sigma + g_{q\delta}\tau_3\delta + g_{q\zeta}\zeta + M_{0_q} + g_{q\Phi}(1-\Phi). \quad (6)$$

We note that for FSUgold only the term with the σ field (with a minus sign) and a large explicit mass term M_{0_B} equal to the nucleon vacuum mass, would be present in Eq. (5). For FSUgold, the contribution of the σ field is zero in the vacuum and decreases the effective mass for finite density. In the chiral SU(3) model, the explicit mass term is much smaller, and the nucleon mass in the vacuum is generated mainly by the σ field (nonstrange chiral condensate). With the increase of density/temperature, the σ field (nonstrange chiral condensate) decreases from its high value at zero density, causing the effective masses of the particles to decrease towards chiral symmetry restoration.

The coupling constants of Eqs. (1)–(6) can be found in Refs. [80,99]. They were chosen to reproduce the vacuum masses of baryons and mesons, nuclear saturation properties, symmetry energy, hyperon optical potentials, and lattice data as well as information about the QCD phase diagram from Refs. [103,104,106,107]. The model reproduces a realistic QCD phase diagram where at the critical end point a first-order PT line begins. The line is calibrated to terminate on the zero temperature axis at 4 times saturation density for charge-neutral β-equilibrated matter. In this way we can reproduce a hybrid star containing a quark core. The behavior of the order parameters and the resulting phase diagrams will be discussed in Sec. VI.

The most important aspect of the chiral SU(3) model is that hadrons are included as quasiparticle degrees of freedom in a chemical equilibrium mixture with quarks. Therefore, the model gives a quasichemical representation of the deconfinement PT (a so-called chemical picture in terms of electromagnetic nonideal plasmas; see, e.g., Ref. [108]). As explained in Sec. II, it is very important for our study that this model contains the right degrees of freedom of low and high densities (namely hadrons and, respectively, quarks) in arbitrary proportions and gives at the same time the deconfinement PT in a "unified EOS" or "single EOS" description.

The assumed full miscibility of hadrons and quarks is, e.g., in contrast to the underlying picture of simple quark-bag models. At sufficiently high temperature, this will also lead to the appearance of quarks soluted in the "hadronic sea," i.e., inside what we call the hadronic (respectively, confined) phase. On the other hand, it is also possible that some hadrons survive being soluted in the "quark sea," i.e., in the quark or deconfined phase. Nevertheless, quarks will always give the dominant contribution in the quark phase and hadrons in the hadronic phase. This is achieved via the field Φ, which assumes nonzero values with the increase of temperature/density and, due to its presence in the baryons' effective masses, suppresses their appearance. On the other hand, the presence of the Φ field in the effective mass of the quarks, included with a negative sign, ensures that they will not be present at low temperatures/densities. The hadronic and the quark phase are characterized and distinguished from each other by their order parameters, whereas Φ is one of them, but also the baryon number density or the asymmetry, as we will show later. The identification of the two phases via order parameters can always be done in an unambiguous way whenever one has phase coexistence. We assume that the interpenetration of quarks and hadrons in the two phases is physical, and it is required to obtain the crossover transition at low baryon chemical potential.

V. THERMODYNAMIC SETUP

A. Definitions

For the (Coulombless) scenarios we are interested in, the following three quantum numbers of each particle species i are relevant: baryon number b_i, electric charge number q_i, and strangeness s_i. The corresponding values can be found in standard textbooks, or, e.g., in Ref. [109]. The quantum numbers of each particle species i also set the total net quantum numbers or total net charges of the thermodynamic system if the total net numbers of particles N_i of each species i are known. The total net number N_i is the difference between the number of particles and the number of corresponding antiparticles of the whole system. The possibly conserved total net quantum numbers (which are extensive) are listed in Table I. Very often, instead of the electric charge number Q, the intensive charge-to-baryon ratio is used, which is defined in the last row of the table. For each of the extensive quantum numbers a corresponding chemical potential can be defined.

TABLE I. Definitions of total net quantum numbers or total net charges which are possibly conserved, depending on the scenario considered, and the corresponding chemical potentials. $F = F(T, V, B, S, Q)$ denotes the total free energy which is a function of temperature T, volume V, and the total net charges B, S, and Q.

Quantity	Definition	Chem. Potential
Baryon number	$B = \sum_i N_i b_i$	$\mu_B = \frac{\partial F}{\partial B}\vert_{T,V,S,Q}$
Strangeness	$S = \sum_i N_i s_i$	$\mu_S = \frac{\partial F}{\partial S}\vert_{T,V,B,Q}$
Electric charge	$Q = \sum_i N_i q_i$	$\mu_Q = \frac{\partial F}{\partial Q}\vert_{T,V,B,S}$
Electric charge fraction	$Y_Q = Q/B$	Not used

TABLE II. Definitions of net quantum numbers or net charges and corresponding chemical potentials of the individual phases inside the phase coexistence region. The free energy F^{I} of phase I is understood as $F^{\mathrm{I}} = F^{\mathrm{I}}(T^{\mathrm{I}}, V^{\mathrm{I}}, B^{\mathrm{I}}, S^{\mathrm{I}}, Q^{\mathrm{I}})$ (analogous definitions for phase II).

Quantity	Definition	Chem. pot.
Baryon number	$B^{\mathrm{I}} = \sum_i N_i^{\mathrm{I}} b_i$	$\mu_B^{\mathrm{I}} = \frac{\partial F^{\mathrm{I}}}{\partial B^{\mathrm{I}}}\vert_{T,V^{\mathrm{I}},S^{\mathrm{I}},Q^{\mathrm{I}}}$
Strangeness	$S^{\mathrm{I}} = \sum_i N_i^{\mathrm{I}} s_i$	$\mu_S^{\mathrm{I}} = \frac{\partial F^{\mathrm{I}}}{\partial S^{\mathrm{I}}}\vert_{T,V^{\mathrm{I}},B^{\mathrm{I}},Q^{\mathrm{I}}}$
Electric charge	$Q^{\mathrm{I}} = \sum_i N_i^{\mathrm{I}} q_i$	$\mu_Q^{\mathrm{I}} = \frac{\partial F^{\mathrm{I}}}{\partial Q^{\mathrm{I}}}\vert_{T,V^{\mathrm{I}},B^{\mathrm{I}},S^{\mathrm{I}}}$
Electric charge fraction	$Y_Q^{\mathrm{I}} = Q^{\mathrm{I}}/B^{\mathrm{I}}$	Not used

These are listed in the third column of Table I. Later we will also use the following chemical potential $\tilde{\mu}$:

$$\tilde{\mu} = \left.\frac{\partial F}{\partial B}\right|_{T,V,S,Y_Q}, \tag{7}$$

$$= \mu_B + Y_Q \mu_Q, \tag{8}$$

which is equal to the Gibbs free energy per baryon (see Appendix D).

For a state which is inside the two-phase coexistence region, two spatially separated macroscopic phases are present. Each phase has its own set of extensive thermodynamic variables and chemical potentials, listed in Table II. The total extensive quantities F, V, B, S, Q, N_i are given as the linear sums of corresponding quantities of the coexisting phases. Particle numbers are connected to particle number densities through the volumes of each phase,

$$\rho_i^{\mathrm{I}} = N_i^{\mathrm{I}}/V^{\mathrm{I}}, \quad \rho_i^{\mathrm{II}} = N_i^{\mathrm{II}}/V^{\mathrm{II}}. \tag{9}$$

B. Scenarios and constraints

Next we are going to define the different cases of the two PTs studied in different physical scenarios. An overview of these scenarios is given in Table III. We consider PTs in three different physical systems: the liquid-gas phase transition of nuclear matter (LG), e.g., in low energy heavy-ion collisions, the deconfinement phase transition in high energy heavy-ion collisions (HI), and the deconfinement phase transition in NS. For the first two scenarios LG and HI we investigate symmetric (S) nuclear matter with $Y_Q = 0.5$ and asymmetric (AS) nuclear matter with $Y_Q = 0.3$. The two different electric charge fractions correspond to heavy-ion reactions of nuclei with different charge-to-mass ratios, Z/A. For ^{197}Au, which is commonly used in heavy-ion experiments, one has $Z/A \simeq 0.4$. However, for peripheral collisions $Y_Q \sim 0.35$ can be reached at certain stages of the evolution, as discussed in Ref. [65]. For all of the asymmetric configurations we also include a forced-congruent (fc) variant of phase equilibrium [52,57,64], where the composition of all conserved charges is forced to be equal in the coexisting phases in frames of Maxwell conditions. In particular, the charge fraction is constrained locally. For the (Coulombless) scenarios of NSs, we investigate the effect of local (NSLCN) and global charge neutrality (NSGCN). Next, we explain the physical meaning of all of the constraints in more detail.

We remark again that we consider only coexistence of macroscopic phases and that we do not consider any Coulomb interactions despite the significant participation of electrically charged particles, as discussed in Sec. II. Nevertheless, the electric charge is an important quantity for our investigations because it is one of the conserved charges which determine the possible noncongruence. Furthermore, the electric charge is also related to isospin. Let us assume that also the total net baryon number B and the total net strangeness S are kept constant, just like in all scenarios of LG and HI. The quantum numbers of the baryons are directly given by the sum of the quantum numbers of their constituent quarks. Therefore, the total net numbers of u, d, and s quarks (free or bound in baryons) are fixed by the total net baryon number B, strangeness S, and electric charge number Q. If the latter three quantities are kept constant, the total quark content does not change, i.e., flavor is conserved. This means no weak reactions occur and also the total isospin of the system is conserved.

In heavy-ion collisions, the typical time scales are on the order of 10^{-23} s, which is much less than weak reaction time scales. Therefore we do not allow for weak reactions in the cases of LG and HI. This is implemented via a fixed value of Y_Q, conservation of baryon number B and conserved total net strangeness $S = 0$. In addition to global conservation of the electric charge in LGS, LGAS, HIS, and HIAS, we also consider locally constrained charge fractions

TABLE III. Constraints and particles used in the six different scenarios. For each particle also the corresponding antiparticle is included. If a quantity of Table II is not listed, its value is not constrained additionally. Note that the combined conservation of B, S, and Y_Q is equivalent to the conservation of baryon number, strangeness, and isospin.

Case	Constraints			Considered particles
LGS	$B = \text{const.}$	$S^{\mathrm{I}} = S^{\mathrm{II}} = 0$	$Y_Q = 0.5$	Neutrons, protons
LGAS	$B = \text{const.}$	$S^{\mathrm{I}} = S^{\mathrm{II}} = 0$	$Y_Q = 0.3$	Neutrons, protons
LGAS_fc	$B = \text{const.}$	$S^{\mathrm{I}} = S^{\mathrm{II}} = 0$	$Y_Q^{\mathrm{I}} = Y_Q^{\mathrm{II}} = 0.3$	Neutrons, protons
HIS	$B = \text{const.}$	$S^{\mathrm{I}} = S^{\mathrm{II}} = 0$	$Y_Q = 0.5$	Baryon octet, quarks
HIAS	$B = \text{const.}$	$S^{\mathrm{I}} = S^{\mathrm{II}} = 0$	$Y_Q = 0.3$	Baryon octet, quarks
HIAS_fc	$B = \text{const.}$	$S^{\mathrm{I}} = S^{\mathrm{II}} = 0$	$Y_Q^{\mathrm{I}} = Y_Q^{\mathrm{II}} = 0.3$	Baryon octet, quarks
NSLCN	$B = \text{const.}$	–	$Y_Q^{\mathrm{I}} = Y_Q^{\mathrm{II}} = 0$	Baryon octet, quarks, leptons
NSGCN	$B = \text{const.}$	–	$Y_Q = 0$	Baryon octet, quarks, leptons

in the forced-congruent cases of LGAS_fc and HIAS_fc. S is set to zero, because initially there is no strangeness in the two colliding nuclei. In principle, there is still the possibility that one has net strangeness in the two phases with $S^{\mathrm{I}} = -S^{\mathrm{II}}$ which is known as strangeness distillation [55]. Here we suppress this degree of freedom to avoid a ternary PT[4] and set $S^{\mathrm{I}} = S^{\mathrm{II}} = 0$ for simplicity. For HIS, HIAS, and HIAS_fc this means that the total number of strange quarks (free or bound in baryons) is equal to the number of antistrange quarks locally and that there is a nonzero strange chemical potential, with two different values in the two phases. For LGS, LGAS, and LGAS_fc strangeness is not relevant at all, because no strange particles are considered but only neutrons and protons. This is appropriate for the typical low energies where the nuclear LGPT is relevant. We do not consider leptons in the cases of LG and HI, because they are not present in the initial configuration and their plasma in the later evolution with equal amounts of particles and antiparticles would not affect the equilibrium conditions between baryons and quarks.

At high temperature, the inclusion of light real mesons, like pions and kaons, is important for some of the thermodynamic quantities (e.g., pressure), since light particles dominate in such regime. However, if their interactions with the baryons are negligible, we do not expect a major influence on the topology of baryonic phase diagrams (e.g., in the temperature-baryon chemical potential plane). In some of the scenarios considered, the meson contribution from the two coexisting phases would cancel exactly or be at least very similar. In this case the inclusion of free mesons would correspond only to a redefinition or shift of some of the thermodynamic quantities. Here we are concentrating on the baryonic component and a more detailed treatment of mesons is postponed to future work.

In cold neutron stars one typically assumes that all possible reactions have reached full equilibrium. Weak reactions do not conserve strangeness and, therefore, it is not listed as a conserved quantity in Table III for the two cases of neutron stars, NSLCN and NSGCN. In principle, weak reactions conserve lepton numbers but in cold neutron stars neutrinos can escape freely and, therefore, the interior lepton numbers are also not conserved.

Finally, electrically charged matter cannot exist in neutron stars on a macroscopic scale, because, otherwise, they would explode, as Coulomb interactions are many orders of magnitude stronger than gravity. Thus, we also include the lepton contribution in form of electrons and muons, which is done easily as they are well described as ideal Fermi-Dirac gases. We implement electric charge neutrality in two different ways, as discussed in the introduction. This is done either via enforced local charge neutrality (NSLCN), where both macroscopic phases are charge neutral and Coulomb forces are absent, or via global charge neutrality (NSGCN) in a Coulombless description, where each of the two phases carries a net electric charge which sum to zero.

We note that the scenarios LG and HI described above could also be taken as simplified examples of supernova matter, for which one has similar values of Y_Q. On the other hand, supernova matter has to be charge neutral, like matter in neutron stars, and, therefore, negatively charged leptons have to be included. For GCN and the Coulombless approximation, charged leptons would not influence the behavior of the PTs in cases of HI and LG. However, for a realistic description of the LGPT in supernovae the Coulombless bulk treatment is not sufficient, and the formation of nuclei and nuclear clusters has to be taken into account, as noted before.

C. Phase and chemical equilibrium conditions

Based on the previous constraints, the equilibrium conditions can be derived. First, we consider the system outside of the phase coexistence region. If there are more particle species than conserved charges, conditions for chemical equilibrium are necessary. The chemical potential μ_i of particle i is related to the chemical potentials of the total charges as follows:

$$\mu_i = b_i \mu_B + s_i \mu_S + q_i \mu_Q, \tag{10}$$

which allows us to calculate the abundances of all particles, if the values of the total charges are known. Note that μ_S is the chemical potential for strangeness as defined in Table I, which differs from the chemical potential of the strange quark. For NSLCN and NSGCN, the nonconservation of strangeness leads to $\mu_S = 0$, which is nothing but the minimization of the thermodynamic potential with respect to strangeness.

We remark that it is also possible to formulate the equilibrium conditions of Eq. (10) by using chemical potentials of three selected particles instead of the chemical potentials μ_B, μ_Q, and μ_S. We want to give an example for this alternative formulation. Taking the chemical potentials of neutrons, protons and lambdas as the basic units, one obtains from Eq. (10)

$$\mu_i = b_i \mu_n + s_i(\mu_n - \mu_\Lambda) + q_i(\mu_p - \mu_n). \tag{11}$$

This sets the chemical potentials of all particles, if μ_n, μ_p, and μ_Λ are determined according to the external constraints (see Table III). For example, this would lead to

$$\mu_u = \tfrac{1}{3}(2\mu_p - \mu_n), \quad \mu_{\Xi^-} = 2\mu_\Lambda - \mu_p. \tag{12}$$

For NSs, where leptons are considered, one would also get

$$\mu_e = \mu_\mu = \mu_n - \mu_p, \tag{13}$$

because of the assumption of nonconservation of the lepton numbers.

Inside the phase coexistence region one has to consider equilibrium conditions between the two phases. Thermal and mechanical equilibrium are given by

$$P = P^{\mathrm{I}} = P^{\mathrm{II}}, \tag{14}$$

$$T = T^{\mathrm{I}} = T^{\mathrm{II}}. \tag{15}$$

Inside each phase, one still has relations analogous to Eq. (10). They give the chemical potential of particle i in phase I (respectively II), expressed by the local chemical potentials of the charges

$$\begin{aligned} \mu_i^{\mathrm{I}} &= b_i \mu_B^{\mathrm{I}} + s_i \mu_S^{\mathrm{I}} + q_i \mu_Q^{\mathrm{I}}, \\ \mu_i^{\mathrm{II}} &= b_i \mu_B^{\mathrm{II}} + s_i \mu_S^{\mathrm{II}} + q_i \mu_Q^{\mathrm{II}}. \end{aligned} \tag{16}$$

[4]With "ternary" we mean that one had three globally conserved charges with three chemical equilibrium conditions.

Next, one has the chemical equilibrium conditions between the two phases. In Coulombless sytems, which are equivalent to terrestrial chemically reacting systems (e.g., Ref. [52]), the local chemical potentials of all species in coexisting phases must be equal, i.e., $\mu_i^{\rm I} = \mu_i^{\rm II}$, if no local constraints are applied, according to the traditional laws of chemical thermodynamics. In this case, $\mu_i^{\rm I} = \mu_i^{\rm II}$ would also follow from $\mu_B^{\rm I} = \mu_B^{\rm II}$, $\mu_Q^{\rm I} = \mu_Q^{\rm II}$, and $\mu_S^{\rm I} = \mu_S^{\rm II}$ and Eqs. (16). However, due to the local constraints applied (see Table III), the interphase chemical equilibrium conditions depend on the scenario considered and have to be derived, e.g., by means of Lagrange multipliers (see also Ref. [64]). In the following, we list the interphase chemical equilibrium conditions for the different cases.

LGS, LGAS, HIS, and HIAS

$$\mu_B^{\rm I} = \mu_B^{\rm II}, \tag{17}$$

$$\mu_Q^{\rm I} = \mu_Q^{\rm II}. \tag{18}$$

Note that $\mu_S^{\rm I} \neq \mu_S^{\rm II}$ in order to have $S^{\rm I} = S^{\rm II} = 0$. In the alternative formulation from above, Eqs. (17) and (18) would be equivalent to

$$\mu_n^{\rm I} = \mu_n^{\rm II}, \tag{19}$$

$$\mu_p^{\rm I} = \mu_p^{\rm II}. \tag{20}$$

NSLCN

$$\mu_B^{\rm I} = \mu_B^{\rm II}, \tag{21}$$

$$\mu_S^{\rm I} = \mu_S^{\rm II} = 0. \tag{22}$$

The latter relation comes from the nonconservation of strangeness and implies that there is a net strangeness in both of the two phases. Note that

$$\mu_Q^{\rm I} \neq \mu_Q^{\rm II}. \tag{23}$$

This means, for example,

$$\mu_p^{\rm I} \neq \mu_p^{\rm II}, \tag{24}$$

$$\mu_e^{\rm I} \neq \mu_e^{\rm II}. \tag{25}$$

We note that according to the Gibbs-Guggenheim conditions (see, for example, Ref. [52]), for a macroscopic equilibrium Coulomb system one should introduce the *electro-chemical* potential [110] $\mu_Q^{*\rm I} = \mu_Q^{\rm I} + V_{\rm Galvani} = \mu_Q^{\rm II} = \mu_Q^{*\rm II}$ (relative to an arbitrary constant in uniform Coulomb systems). With this description, the generalized electrochemical potentials of all charged particles would be equal in the two coexisting macroscopic phases, but this is not used here.

NSGCN

$$\mu_B^{\rm I} = \mu_B^{\rm II}, \tag{26}$$

$$\mu_S^{\rm I} = \mu_S^{\rm II} = 0, \tag{27}$$

$$\mu_Q^{\rm I} = \mu_Q^{\rm II}. \tag{28}$$

So here we have

$$\mu_p^{\rm I} = \mu_p^{\rm II}, \tag{29}$$

$$\mu_e^{\rm I} = \mu_e^{\rm II}. \tag{30}$$

LGAS_fc and HIAS_fc. Next, we give the equilibrium conditions if the local charge fractions are constrained to have the same value, $Y_Q^{\rm I} = Y_Q^{\rm II}$ $(= Y_Q)$. Because in the considered cases only baryon number remains as a globally conserved charge, the Maxwell construction for a congruent PT can be used. It is well known that for the "Maxwell" phase transition in a neutron star with local charge neutrality and β equilibrium the baryon chemical potential, which in this case is equivalent to the neutron chemical potential, has to be equal in the two phases, see Eq. (21). For HIAS one obtains instead the following interphase chemical equilibrium condition [64]:

$$\tilde{\mu}^{\rm I} = \tilde{\mu}^{\rm II}, \tag{31}$$

$$\Leftrightarrow \mu_B^{\rm I} + Y_Q \mu_Q^{\rm I} = \mu_B^{\rm II} + Y_Q \mu_Q^{\rm II}, \tag{32}$$

with the local Gibbs free energy per baryon,

$$\tilde{\mu}^{\rm I} = \left.\frac{\partial F^{\rm I}}{\partial B^{\rm I}}\right|_{T, V^{\rm I}, S^{\rm I}, Y_Q^{\rm I}}, \tag{33}$$

$$= \mu_B^{\rm I} + Y_Q^{\rm I} \mu_Q^{\rm I}, \tag{34}$$

and the analogous expression for $\tilde{\mu}^{\rm II}$ of phase II. Equation (31) expresses the equality of the specific Gibbs free energy of the two phases, respectively the Gibbs free energy per baryon used here (see Appendix D). This is merely the standard Maxwell construction for a congruent PT, which is also applicable for the forced-congruent case.

In general, the baryon and charge chemical potentials will not be the same for the two phases in the phase coexistence region, because Eq. (32) is the only chemical equilibrium condition for the cases LGAS_fc and HIAS_fc. For a better comparison with the noncongruent variants LGAS and HIAS, we will show the phase diagrams of LGAS, LGAS_fc, HIAS, and HIAS_fc not only as a function of μ_B but also as a function of $\tilde{\mu}$.

Total chemical potentials inside the two-phase mixture. The equilibrium conditions given above allow one to determine the phase boundaries and fully specify the properties of the two phases in equilibrium. However, the nonequality of local chemical potentials due to local constraints leads to the following complication: in this case, it is not obvious how the total chemical potentials of the charges in the two-phase mixture (defined analogously to the ones in Table I, with the local constraints of Table III in addition) are related to the local chemical potentials of Table II, which can have different values in the two phases. These relations are derived in Appendix C. We are not aware that these expressions have been published in the literature before.

VI. RESULTS OF CALCULATIONS

In this section we are showing the results for the phase diagrams of each case studied, whereas we begin with the LGPT and continue with the QHPT.

A. Nuclear liquid-gas phase transition

Figure 1 shows the phase diagram of the case of LGS, i.e., for the liquid-gas phase transition of symmetric nucleonic matter. In principle, symmetric nuclear matter is a two-component, binary system of protons and neutrons (respectively, baryon

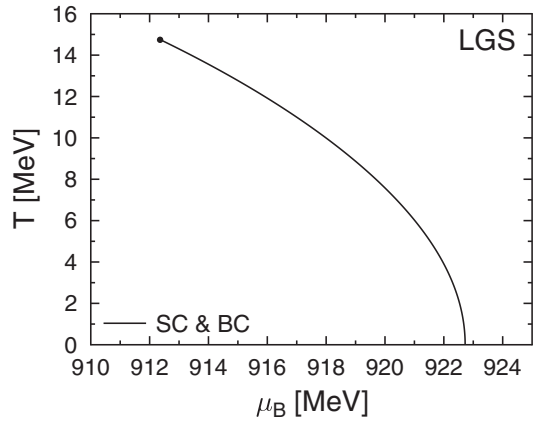

FIG. 1. Phase diagram in the temperature-baryon chemical potential plane for the case of LGS ($Y_Q = 0.5$). The saturation curve (SC) coincides with the boiling curve (BC). The black dot marks the ordinary VdW-like critical point (CP).

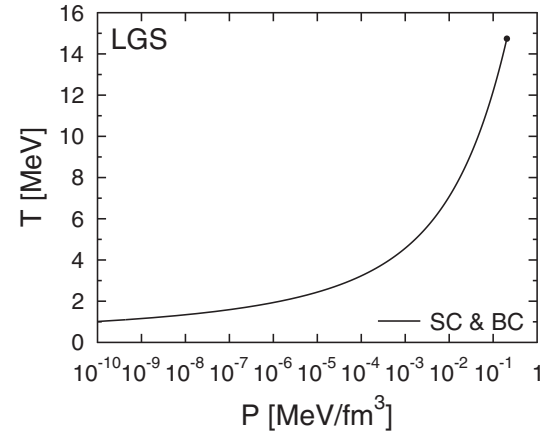

FIG. 2. Phase diagram in the temperature-pressure plane for the case of LGS; otherwise, the same notation and depiction as in Fig. 1 is used.

number and isospin). However, the nuclear interactions and isospin symmetry lead to azeotropic behavior, i.e., the ratio of protons to neutrons does not change during phase coexistence and the two coexisting phases remain symmetric. The electric charge chemical potential μ_Q of symmetric nuclear matter is zero, independently of density and temperature. Therefore, no isospin distillation occurs, i.e., there is no transfer of isospin per baryon, respectively, Y_Q, between the two phases. Since $\mu_Q \equiv 0$, the relation of chemical equilibrium with respect to changes of Y_Q, Eq. (18), is automatically fulfilled, and only Eq. (17) carries relevant information. Consequently, symmetric nuclear matter behaves like a unary system and the PT is of congruent type with a phase-coexistence line in the T-μ_B plane, shown in Fig. 1. This line can be obtained with a Maxwell construction by the corresponding constraints of Sec. V C. Note that the saturation curve (SC) (which is also called "dew-point line") and the boiling curve (BC) (which is also called "bubble-point line") coincide in the case of congruent PTs or azeotropic compositions and are split into separate boundaries in the general case of NCPT. The critical point (CP) marked by the black dot, which is also a (critical) end point here, is located at a temperature of 14.75 MeV and baryon chemical potential of 912.4 MeV (further values are given in Table IV). It is known from other studies that the CP of LGS is usually also the global maximum

TABLE IV. Approximate location of the critical and pseudocritical points of the different scenarios.

Case	T (MeV)	ρ_B (fm^{-3})	μ_B (MeV)	p (MeV/fm^3)
LGS	14.75	0.046	912.4	0.205
LGAS	13.99	0.049	927.4	0.241
LGAS_fc	12.68	0.044	928.3	0.171
HIS	165.5	0.24	383	73.1
HIAS	165.3	0.22	381	68.6
HIAS_fc	156.5	0.44	611	95.8
NSLCN	168.6	0.16	247	162.8
NSGCN	168.9	0.14	224	161.1

of the phase transition temperature, i.e., for all possible values of Y_Q.

In Fig. 2 we show the pressure-temperature phase diagram, where we also obtain a phase transition line. Note that the pressure on the coexistence line goes to zero in the zero-temperature limit. For a congruent PT the Clapeyron equation is valid,

$$\frac{dP}{dT} = \frac{s^{\mathrm{I}} - s^{\mathrm{II}}}{1/\rho_B^{\mathrm{I}} - 1/\rho_B^{\mathrm{II}}}, \tag{35}$$

with $s^{\mathrm{I}} = S^{\mathrm{I}}/B^{\mathrm{I}}$ and $s^{\mathrm{II}} = S^{\mathrm{II}}/B^{\mathrm{II}}$ denoting the entropy per baryon of the two phases. The Clapeyron equation describes how the slope of the pressure-temperature phase transition line is related to the difference in baryon number density and entropy per baryon of the two phases. In our investigation, we always have $\rho_B^{\mathrm{I}} < \rho_B^{\mathrm{II}}$, i.e., the first phase is assumed to have lower density. In Fig. 2 we see that $dP/dT > 0$, and, thus, $s^G > s^L$ (where we have replaced "I" with "G" and "II" with "L"). The gas phase has a higher entropy per baryon and is always less dense than the liquid phase, which is a characteristic of the LGPT.

In Fig. 3 the binodal region is shown in the temperature-density plane. The gray line to the left of the critical point depicts the SC, where droplets of liquid form within the nucleon gas. The black line is the BC, where bubbles of gas form inside the liquid. The region enclosed by the two lines is the phase coexistence region, where a two-phase mixture of gas and liquid is present. Here, and also in all following plots, filled areas correspond to states of such a two-phase coexistence. Due to the congruent behavior of LGS, for each point inside the binodal or phase coexistence region, the gas state on the SC is in coexistence with the liquid state on the BC at the same common temperature. Thus, the gas and the liquid are distinguished from each other by density, whereas the liquid is always more dense. At the critical point the two phases are identical. Inside the phase coexistence region, the volume fraction of the liquid phase $\alpha = V^L/V$ and the gas phase $(1 - \alpha)$ are set by the total baryon number density $\rho_B = B/V$

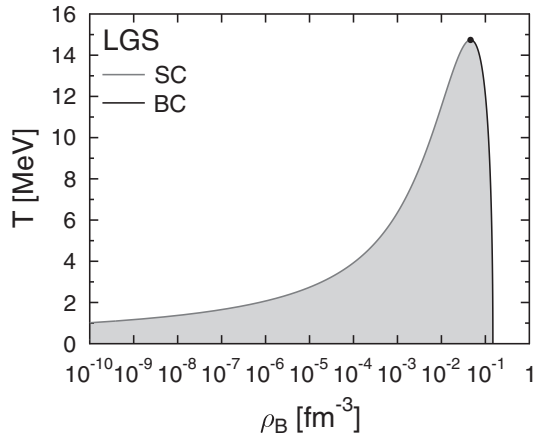

FIG. 3. The binodal line which encloses the coexistence region (filled with gray) in the T-ρ_B plane for the case of LGS. The black dot marks the critical point (CP). The gray line to the left of the CP is the saturation curve (SC), and the black line to the right is the boiling curve (BC).

through

$$\rho_B = \rho_B^G(1-\alpha) + \rho_B^L\alpha. \tag{36}$$

Obviously, one has $\alpha = 0$ on the SC and $\alpha = 1$ on the BC.

For asymmetric nuclear matter in the case of LGAS one obtains a noncongruent phase transition, which can be seen in Fig. 4, depicted by the orange (light gray) and blue (dark gray) thick lines. For the nontrivial solution of the equilibrium conditions in the noncongruent case we have used the method described in Ref. [44]. The gray and black thin lines show the forced congruent variant LGAS_fc which will be discussed later. For LGAS one has a phase coexistence region in T-μ_B, enclosed by the orange (light gray) and blue (dark gray) thick lines, instead of a single line as in Fig. 1 for LGS. Also, in all following plots, we will use colored thick lines for NCPTs. Thus, one can also distinguish between the branch belonging to the SC and the branch belonging to the BC by different colors.

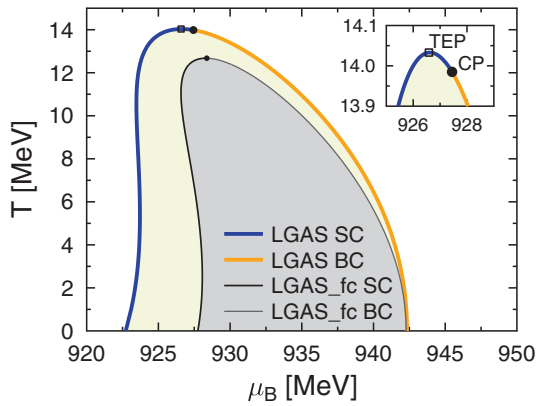

FIG. 4. (Color online) Phase diagram in the temperature-baryon chemical potential plane for the two asymmetric systems LGAS and LGAS_fc with $Y_Q = 0.3$. The gray and black thin lines show the forced-congruent variant LGAS_fc, and the corresponding small black dot is the pseudocritical point. The colored thick lines depict the case of LGAS, where Y_Q is not constrained locally. The corresponding black dot is the critical point and the open square the temperature end point. The inlay shows a close-up to the region around the critical point (CP) and temperature end point (TEP) of the noncongruent case of LGAS. The filled areas are the coexistence regions.

As was stressed in Refs. [52,61], in noncongruent VdW-like phase transitions of gas-liquid type there is no longer a unique "critical end point." Instead, three separate end points exist: maximal temperature (cricondentherm),[5] maximal pressure (cricondenbar),[6] and point of extremal chemical potential.[7] In NCPT, these three "topological" end points are separated from the singular thermodynamic object—the true noncongruent critical point.[8] Note also that the critical point of a congruent phase transition is determined by

$$\left.\frac{\partial P}{\partial \rho_B}\right|_T = \left.\frac{\partial^2 P}{\partial \rho_B^2}\right|_T = 0. \tag{37}$$

In contrast, for a NCPT this criteria is not applicable, and the critical point does not fulfill it in general.

The inlay of Fig. 4 shows that the temperature end point differs from the critical point. For LGAS, the critical point is found at $T^{\rm CP} = 13.99$ MeV (lower than in LGS) and $\mu_B^{\rm CP} = 927.4$ MeV. It is very interesting that this reduction of the critical temperature agrees very well with the experimental results of Refs. [47]. The further properties of the critical point are given in Table IV. The temperature end point is located at $T^{\rm TEP} = 14.03$ MeV and $\mu_B^{\rm TEP} = 926.6$ MeV. We remark that for LGAS the temperature end point is located on the saturation curve [blue (dark gray) thick line], which, in principle, could also be located on the boiling curve [orange (light gray) thick line]. This topology (i.e., location of the temperature end point on the two-phase boundary relative to the critical point) is the same as for the gas-liquid NCPT in uranium-oxygen plasma [57–62], which is taken as the prototype of NCPT for the present study of LGAS (compare Figs. 5 and 6 with Fig. 1 of Ref. [52]).

In LGAS_fc the two phases are constrained locally to have the same charge fraction $Y_Q^G = Y_Q^L = 0.3$. The results are depicted by the gray and black thin lines in Fig. 4. The two lines also enclose a phase coexistence region, which illustrates the nonequality of μ_B of the two phases in the phase coexistence region, due to the locally constrained charge fraction (see also the discussion in Sec. V C and Appendix C 1). The Gibbs free

[5]The temperature end point (TEP) or point of maximal temperature, which is also called the "cricondentherm" [54,111], is defined as the point with the highest temperature where phase coexistence is possible.

[6]The pressure end point, also called the "cricondenbar" [54,111], is defined as the point on the binodal where the maximal pressure is obtained.

[7]The chemical potential end point or point of extremal chemical potential is defined as the point where the chemical potential of the binodal surface is extremal with respect to temperature.

[8]The critical point is defined as the point on the binodal surface where the two phases are identical. Because it is located on the binodal, an infinitesimal change of the state can lead to phase separation into two phases which can be distinguished from each other by an order parameter.

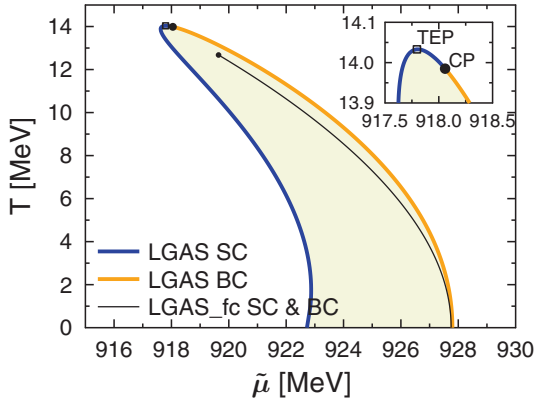

FIG. 5. (Color online) Phase diagram in the plane of temperature and Gibbs free energy per baryon $\tilde{\mu}$ for the cases of LGAS and LGAS_fc ($Y_Q = 0.3$). Otherwise, the same notation and depiction as in Fig. 4 are used.

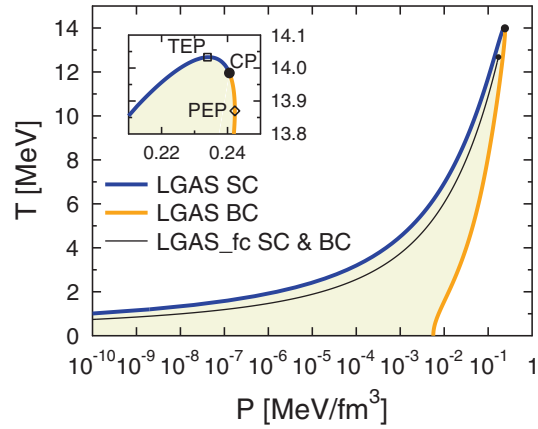

FIG. 6. (Color online) Phase diagram in the plane of temperature and pressure for the cases of LGAS and LGAS_fc ($Y_Q = 0.3$). In addition to the critical point (black dot), the temperature (open square) and pressure end points (open diamond) are shown in the inlay. Otherwise, the same notation and depiction as in Fig. 4 are used.

energy per baryon $\tilde{\mu}$ is the only chemical potential which is equal in the two phases. Furthermore, for isothermal phase transitions it is a constant, because the properties of the two phases do not change. In contrast to the noncongruent phase transition LGAS, for the forced-congruent phase transition LGAS_fc μ_B is dependent on the baryon number density ρ_B and given by

$$\mu_B = \mu_B^G \frac{\rho_B^G}{\rho_B}(1-\alpha) + \mu_B^L \frac{\rho_B^L}{\rho_B}\alpha, \tag{38}$$

which is derived in Appendix C 1.

The phase diagrams as a function of the Gibbs free energy per baryon $\tilde{\mu}$ are shown in Fig. 5 for the cases of LGAS and LGAS_fc. The banana-shaped region of LGAS is typical for noncongruent liquid-gas-like phase transitions, see Refs. [57–62]. In Fig. 5 the congruence of LGAS_fc becomes obvious. Comparing LGAS and LGAS_fc, the phase coexistence region turns into a phase coexistence line, when enforcing the local constraint for the charge fraction. Furthermore, for LGAS_fc the pseudocritical point (properties listed in Table IV) coincides with the temperature and chemical potential end points. Note that the pseudocritical point of a forced-congruent phase transition obeys Eq. (37). We remark that the phase transition line of the forced-congruent variant must lie strictly inside the two-phase region of the noncongruent phase transition [57–62], which also can be seen as a consequence of Le Chatelier's principle. As an exception, both objects could touch each other in azeotropic points of the parameter space, as seen for LGS.

Note that for the case of LGS, $\mu_B = \tilde{\mu}$, since $\mu_Q \equiv 0$. Thus, the phase-coexistence line of LGAS_fc in Fig. 5 can be directly compared with the one of LGS in Fig. 1 and it is found that their shape is very similar. However, states on the phase coexistence line of LGAS_fc in Fig. 5 belong to two different values of the baryon chemical potential, shown by the two gray and black thin lines in Fig. 4. If $\tilde{\mu}$ in LGAS_fc were changed in a continuous way and the phase transition line in Fig. 5 is crossed, μ_B jumps from the value of the gas phase to the value of the liquid phase in Fig. 4. This can be seen as a sign of the *enforced* congruence, in contrast to the azeotropic congruent phase transition LGS.

Figure 6 shows the same scenarios as in the previous figures but gives the phase diagrams in the temperature-pressure plane. Here it is clear that the phase transition in the forced congruent variant LGAS_fc occurs only at a single value of the pressure, which is the same behavior as in Fig. 2 for LGS. In contrast, for a given temperature in LGAS, there is an extended coexistence range in pressure, which is enclosed by the SC and BC. The names "SC" and "BC" are widely accepted for noncongruent evaporation in chemically reacting plasmas [57–61] where their meaning is obvious. They are also most intuitive for LGAS for this kind of phase diagram: For a fixed pressure of, e.g., 10^{-2} MeV/fm^3 and starting from $T = 0$, by heating the system one will reach the boiling curve, where bubbles of gas appear inside the liquid. Conversely, if one starts at high temperatures and cools the system isobarically, droplets of liquid will form within the gas when the saturation curve is reached. In this figure we can also identify the pressure end point which is located on the BC of LGAS. In the gas-liquid NCPT in uranium-oxygen plasma [57–62], which is the prototype for our present study of NCPT in LGAS, one has the same topology that the pressure end point is located on the BC, despite differences in the thermodynamic variables by many orders of magnitude (compare Fig. 6 with Fig. 1 in Ref. [52]). For LGAS_fc, all three end points coincide with the critical point defined by Eq. (37) (see Fig. 1 in Ref. [52]).

In spite of the similarity of the NCPT in LGAS with its terrestrial prototypes [57–62], the significant difference in the topology of P-T diagrams should be stressed (compare Fig. 6 above with Fig. 1 in Ref. [52]). While the pressure on both boundaries of the noncongruent PT in the uranium-oxygen system [57–62]—boiling and saturation curves—tends to zero for the limit $T \to 0$, the pressure on the boiling curve in NCPT in asymmetric ($Y_Q = 0.3$) LGPT does not tend to zero when $T \to 0$ in our case (see Fig. 6). The same feature was noted already for the NCPT of asymmetric nuclear matter calculated with a different EOS (Fig. 3 in Ref. [112]). The reason for

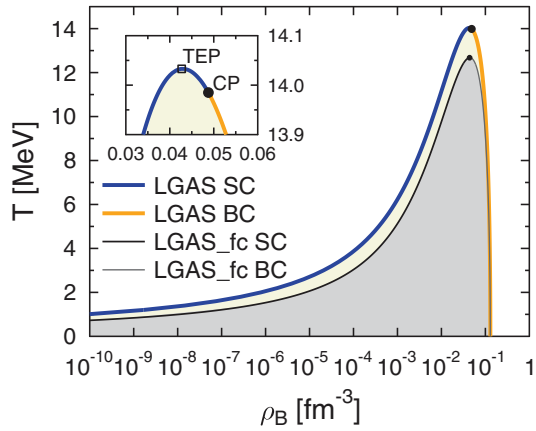

FIG. 7. (Color online) The binodal line enclosing the coexistence region in the T-ρ_B plane for LGAS and LGAS_fc ($Y_Q = 0.3$). Otherwise, the same notation and depiction as in Fig. 4 are used.

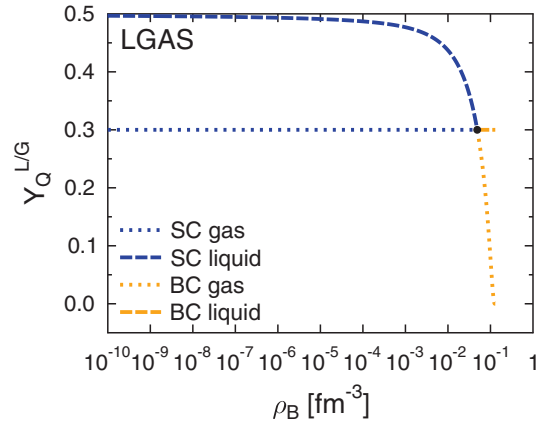

FIG. 8. (Color online) The charge fraction of the liquid (dashed lines) and the gas phase (dotted lines) for the case of LGAS as a function of the coexistence density ρ_B along the binodal line of Fig. 7. The blue (dark gray) lines show the charge fractions of the two coexisting phases for states on the saturation curve presented in previous figures, the orange (light gray) lines for states on the boiling curve.

this feature is the difference in the physical nature of the involved forces which are relevant for the noncongruence in a chemically reacting uranium-oxygen plasma [57–62] and in asymmetric nuclear matter and the use of Fermi-Dirac statistics for the latter.

In Fig. 7 we show the binodal or phase coexistence regions for LGAS and LGAS_fc in the temperature-density plane, similarly as in Fig. 3 for LGS. Again, the noncongruent behavior of LGAS can be identified by the nonequivalence of the temperature end point and the critical point. Conversely, for LGAS_fc the end points and the (pseudo-) critical point coincide. Furthermore, for isothermal processes of LGAS at temperatures $T^{\rm CP} < T < T^{\rm TEP}$ so-called retrograde condensation occurs (see also Refs. [42,43]): Imagine, e.g., an isothermal compression at $T = 14$ MeV. First, one hits the saturation curve from the left, and a liquid with a larger Y_Q and a larger ρ_B appears inside the gas phase. With increasing density, the volume fraction of the liquid will, first, increase. But for retrograde condensation, for densities larger than a certain density, the volume fraction will decrease again, until it returns to zero at the right side of the saturation curve. The liquid has disappeared again after the phase coexistence region has been crossed.

The noncongruent behavior of LGAS is further analyzed in the following plots of local "chemical" composition and density. Figure 8 shows the charge fractions of the two phases which are in coexistence, if one moves along the liquid and vapor binodal lines of Fig. 7. The blue (dark gray) dotted line "SC gas" in Fig. 8 depicts the charge fraction of the gas phase Y_Q^G for the states on the saturation curve shown in Fig. 7. On the saturation curve, the gas phase is in coexistence with a liquid phase which has a different charge fraction Y_Q^L, shown by the dashed blue (dark gray) line. Moreover, for the conditions of the boiling curve of Fig. 7, we always have coexistence of a gas phase [orange (light gray) dotted line in Fig. 8] with a liquid phase [orange (light gray) dashed line in Fig. 8], which have different charge fractions.

In all previous plots, the depicted quantities correspond to total thermodynamic quantities, i.e., of the system as a whole. In contrast, in Figs. 8–10 we are showing individual properties of the two coexisting phases. Now and in the following we are using dashed and dotted lines in such plots to illustrate this difference. The color coding helps to identify the same states in the different diagrams. For example, in Fig. 8, the ends of the orange (light gray) curves, which correspond to $T = 0$, are given by the highest density of coexistence of LGAS in Fig. 7, which is on the orange (light gray) solid line.

In Fig. 8, one of the two phases always must have $Y_Q = 0.3$, whereas the charge fraction of the second phase is not constrained, because its volume fraction is still zero on the binodal line. For states on the saturation curve one is still in the gas phase, i.e., $\alpha = 0$, thus, $Y_Q^G = 0.3$. For states on the boiling curve one is still in the liquid phase, $\alpha = 1$, and $Y_Q^L = 0.3$. The charge fraction is an order parameter for LGAS and, thus, it can be used to characterize the two phases, with the identification that the gas phase always has a lower charge fraction than the liquid, i.e., $Y_Q^G < Y_Q^L$. Only at the critical

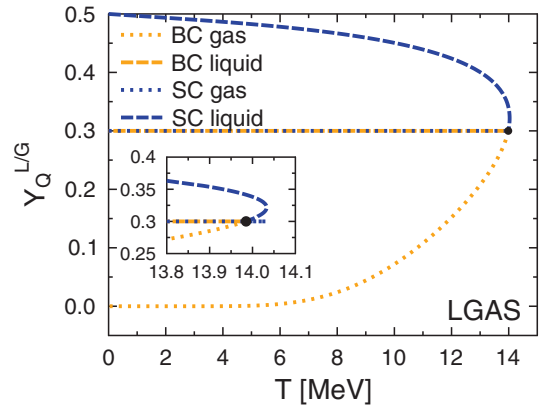

FIG. 9. (Color online) As shown in Fig. 8 but now in dependence of the coexistence temperature of the binodal line of Fig. 7. The inlay shows a close-up of the region around the critical point, including the region of so-called retrograde condensation at $T > T^{\rm CP}$.

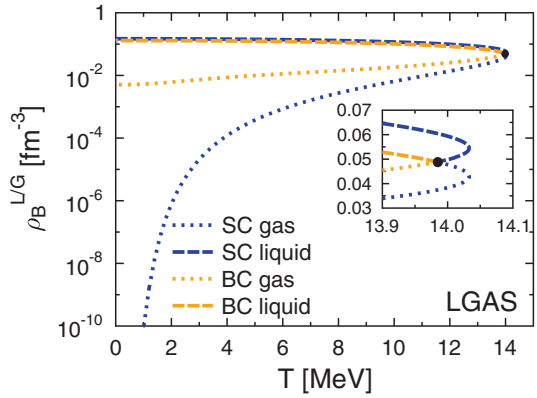

FIG. 10. (Color online) The baryon number density of the liquid (dashed lines) and the gas phase (dotted lines) for the case of LGAS as a function of the coexistence temperature on the binodal line of Fig. 7. Otherwise, the same notation and depiction as in Fig. 9 are used.

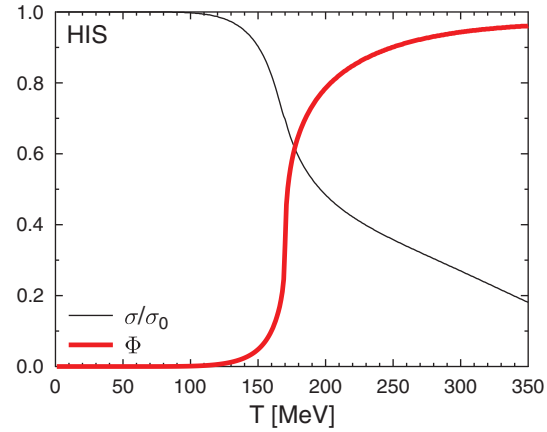

FIG. 11. (Color online) Order parameter for chiral symmetry restoration/breaking σ normalized by the vacuum value σ_0 and order parameter for deconfinement/confinement Φ versus temperature at zero baryon chemical potential for symmetric matter of the case of HIS ($Y_Q = 0.5$).

point is equality established, $Y_Q^G = Y_Q^L$. It is interesting to note that the charge fraction of the phase with $Y_Q \neq 0.3$ shows the same dependence on density before and after the critical point.

In Fig. 9 we also show the charge fractions of the two phases along the binodal line but now as a function of the coexistence temperature. By comparison with Figs. 4–7, it is obvious that for each coexistence temperature there are always two points on the binodal line, corresponding to two different halves of the binodal line which are separated from each other by the temperature end point. For each half, two phases with different values of Y_Q are in coexistence. Consequently, in Fig. 9, for each temperature there are always four values of Y_Q. For $T < T^{\rm CP}$, one has $Y_Q^G = 0.3$ and $Y_Q^L > 0.3$ on the saturation curve and $Y_Q^G < 0.3$ and $Y_Q^L = 0.3$ on the boiling curve. Note that the two lines with $Y_Q = 0.3$ are on top of each other. For $T^{\rm CP} < T < T^{\rm TEP}$, both halves belong to the saturation curve, and, thus, $Y_Q^G = 0.3$ for both halves, each being in coexistence with a different configuration of the liquid with $Y_Q^L > 0.3$.

The previous two figures can be used to identify the high degree of isospin distillation of LGAS in the limit $T \to 0$. Let us consider a decompression at $T \sim 0$ of the asymmetric system with $Y_Q = 0.3$. Once the boiling curve is reached, vapor bubbles appear which in this case consist of pure neutron gas, $Y_Q^G \to 0$. Obviously, this leads to the distillation of a symmetric liquid by evaporation of pure neutron bubbles from a boiling asymmetric liquid phase. On the other hand, for saturation conditions ("dew point") at $T \sim 0$, liquid microdrops tend to the exactly symmetric composition, $Y_Q^L \to 0.5$. These features of the NCPT of the case of LGAS differ significantly from the behavior of the chemical composition (O/U ratio) in NCPTs of uranium-oxygen systems (compare Fig. 9 with Fig. 2 of Ref. [57] and Fig. 3 of Ref. [58]).

In a similar way as in Fig. 9, in Fig. 10 we show the baryon number densities of the two phases for each of the two halves of the binodal line as a function of the coexistence temperature. Presented in this way, one sees that the density is also an order parameter of LGAS, whereas the liquid is the phase with the higher density. At the critical point, the liquid and the gas have the same density and charge fraction and, thus, can no longer be distinguished from each other. The discussion of this figure is similar to that for Fig. 9: For $T < T^{\rm CP}$ there are the ρ_B curves from the liquid [blue (dark gray) dashed line] and the gas [blue (dark gray) dotted line] on the saturation curve and another pair of ρ_B curves from the liquid [orange (light gray) dashed line] and the gas [orange (light gray) dotted line] on the boiling curve. For $T^{\rm CP} < T < T^{\rm TEP}$ there are still the four different values of ρ_B. However, now all points belong to the saturation curve.

B. Deconfinement phase transition

For the LGPT we used the baryon number density and charge fraction as order parameters. For the deconfinement and chiral symmetry PTs, typically the Polyakov loop Φ and the chiral condensate σ are used, as already discussed in Sec. IV. The field σ characterizes chiral symmetry restoration, whereas Φ can be taken as a measure for deconfinement. At finite temperature and $\mu_B = 0$ (respectively $\rho_B = 0$),[9] there is no first-order PT but a smooth crossover between the hadronic (confined, chiral symmetry broken) and the quark phase (deconfined, chiral symmetry partly restored) [106]. This is shown in Fig. 11 for HIS, where the ratio σ/σ_0 decreases from one to lower values and Φ goes from zero to a value close to one in a smooth fashion. We remark that we define the crossover temperature $T^{\rm co}$ as the peak of the change of the chiral condensate and Φ with T, yielding a value of $T^{\rm co} = 171$ MeV, in accordance with lattice QCD results [107]. This behavior of the order parameters corresponds to the

[9] We remind the reader that we include antiparticles, therefore if $T > 0$, we have equivalence between $\rho_B = 0$ and $\mu_B = 0$. Furthermore, for $T > 0$, $\mu_B < 0$ corresponds to net antimatter with $\rho_B < 0$, which is not relevant here. For $T = 0$ the situation is a bit more complicated, because of the LGPT which extends down to $\rho_B = 0$ at a constant finite value of μ_B.

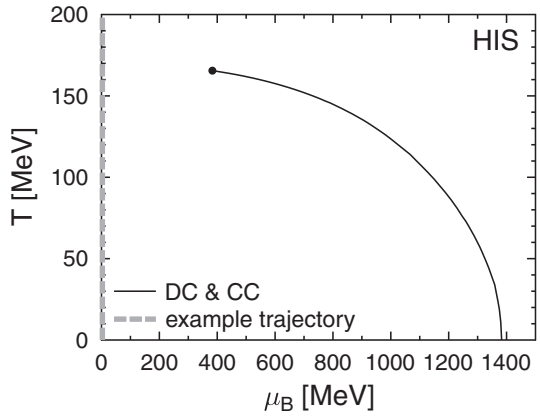

FIG. 12. Phase diagram in the temperature-baryon chemical potential plane for the case of HIS ($Y_Q = 0.5$), for which the deconfinement curve (DC) coincides with the confinement curve (CC). The black dot marks the critical point. The thick gray line along the ordinate shows part of the example trajectory belonging to Fig. 11.

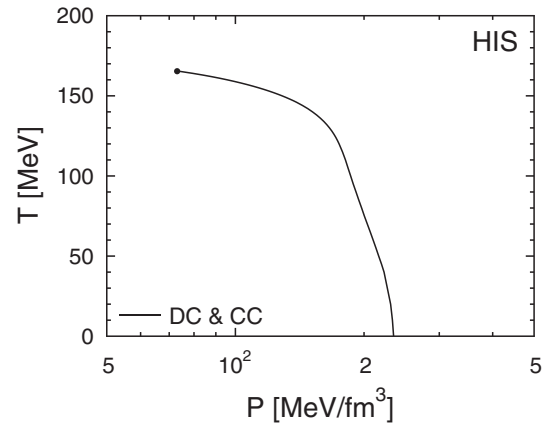

FIG. 13. Phase diagram in the temperature-pressure plane for the case of HIS. Otherwise, the notation and depiction are as in Fig. 12.

example trajectory through the phase diagram of HIS shown in Fig. 12.

For high-enough baryon number densities, the QHPT turns into a first-order phase transition. This can be seen in Fig. 12, where we show the first-order phase transition line for the case of HIS, i.e., for heavy-ion collisions of symmetric nuclei. The critical point is located at $T^{\rm CP} = 165.5$ MeV and $\mu_B^{\rm CP} = 383$ MeV, again, in accordance with lattice QCD results [107]. Its further properties are listed in Table IV. The topology of this PT is the same as in LGS, see Fig. 1, only the typical scales differ. For example, the critical point of HIS is at a roughly 10 times higher temperature. For the QHPT, we will use the terms "deconfinement curve" (DC) instead of "saturation curve" and "confinement curve" (CC) instead of "boiling curve," which we think is more meaningful. If coming from low densities and temperatures, first, droplets of denser deconfined quark matter will appear when the DC is reached. Conversely, if coming from high densities and temperatures, when the CC is reached, the first quarks will start to be confined into bubbles of less dense hadronic matter. There is an interesting analogy to the "ionization boundary curve" and "recombination boundary curve" of the hypothetical ionization-driven plasma phase transition in dense hydrogen at the megabar pressure range (see, e.g., Refs. [113–115]). This first-order PT in weakly ionized hydrogen (predominantly H and H_2 and small amount of p and e) is driven by a jumplike ionization (deconfinment) into highly ionized hydrogen (predominantly p and e and small amount of H and H_2). We want to point out the similarity between the hydrogen plasma which is an arbitrary solution of H_2, H, p, and e and the chiral SU(3) model in which quarks and hadrons can in principle also be mixed in arbitrary proportions (nevertheless, a clear distinction of the two phases is always possible, see Sec. IV).

HIS is, in principle, a binary system, with baryon number and electric charge (respectively isospin) as two globally conserved charges (see Table III). But the PT in HIS is azeotropic, meaning it is congruent and the Maxwell construction can be used, just like symmetric nucleonic matter in LGS. It is not so obvious as for LGS that matter in HIS is an azeotrope, because a whole set of particles, including strange ones, is considered (see Table III). However, strange quarks and hyperons do not invalidate the relation between isospin symmetry and azeotropic behavior, if strangeness is set locally to zero, as is done here. In this case, the total density of strange quarks, i.e., in form of unbound strange quarks or bound in hyperons, is equal to the total density of antistrange quarks. A more detailed explanation of the matter is given in Appendix B.

In Fig. 13 the phase diagram in the pressure-temperature plane is depicted. Comparing with Fig. 2 one realizes an important difference between the QHPT and the LGPT: The slope of the phase transition line is negative. Therefore, the QHPT is not of liquid-gas type. With the Clapeyron equation (35) one finds that this is due to the fact that the hadronic phase, which is less dense, has a lower entropy per baryon than the quark phase, $s^H < s^Q$ (where we have replaced "I" with "H" and "II" with "Q"), which is opposite to the behavior in the LGPT. The negative slope of the p-T phase diagram makes the QHPT fundamentally different from the LGPT. This fact (negative slope of the p-T boundary for QHPT in a symmetric system) is not absolutely new (e.g., presentations by I.I. at several conferences[10] and discussion in Ref. [115]; L. Satarov, private communication (2010), based on calculations via EOS model described in Ref. [116]; J. Randrup, presentations at several conferences[11] and Ref. [117] and Ref. [118]) but is not well recognized yet. Further investigation and analysis of this fundamental difference between the LGPT and QHPT is in preparation [119]. Figure 14 shows the coexistence region in the temperature-baryon number density plane, in a similar way to Fig. 3 for the LGPT. Note that the shape of the phase coexistence region of HIS differs from that of LGS. This is, once more, a manifestation (and not the last one) of the fundamental difference between the LGPT and QHPT.

In the case of heavy-ion collisions with asymmetric Coulombless matter (HIAS), one has a true binary system.

[10] See, e.g., http://theor.jinr.ru/~cpod/Talks/240810/Iosilevskiy.pdf.
[11] See, e.g., http://theor.jinr.ru/~cpod/Talks/260810/Randrup.pdf.

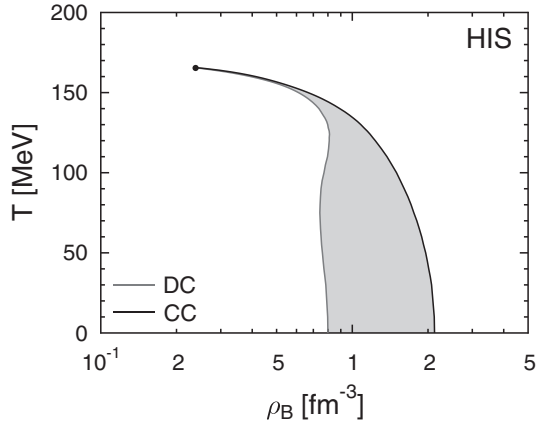

FIG. 14. Phase diagram in the temperature-baryon number density plane for the case of HIS. The deconfinement curve (DC) is to the left of the confinement curve (CC). The gray area shows the two-phase coexistence region. Otherwise, notation and depiction as in Fig. 12.

The PT is noncongruent and the Gibbs construction must be used. This is visible in Fig. 15, where one obtains a phase-coexistence region instead of a phase-transition line as in HIS before. We can compare HIAS with LGAS of Fig. 4. Obviously, the phase-coexistence region is much narrower than for LGAS if we compare the width in μ_B relative to the extension in temperature. HIAS_fc is the forced congruent variant, where the charge fraction is constrained locally, $Y_Q^H = Y_Q^Q = 0.3$, so the Maxwell construction can be used. The gray thin line is the corresponding DC, and the black thin line the CC, which partly covers the CC of HIAS. Very interestingly, the DC and CC changed order for HIAS_fc compared to HIAS. We will explain this interesting result in detail later.

The phase diagrams as a function of the Gibbs free energy per baryon $\tilde{\mu}$ are shown in Fig. 16 and as a function of pressure

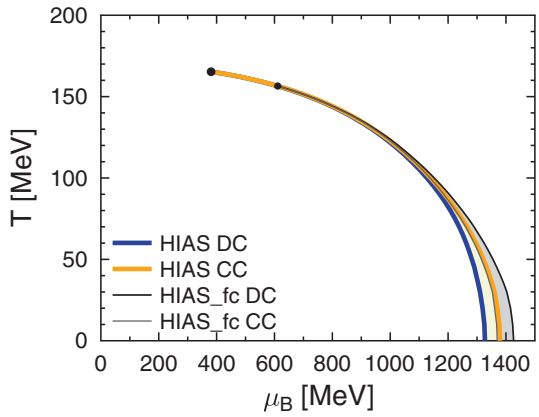

FIG. 15. (Color online) Phase diagram in the temperature-baryon chemical potential plane for the cases of HIAS and HIAS_fc ($Y_Q = 0.3$). The colored thick lines belong to HIAS, the gray and black thin ones to HIAS_fc. The large black dot marks the critical point of HIAS and the small black dot the pseudocritical point of HIAS_fc. The filled areas show the coexistence regions. Note that for HIAS_fc the confinement curve (CC) is to the left of the deconfinement curve (DC).

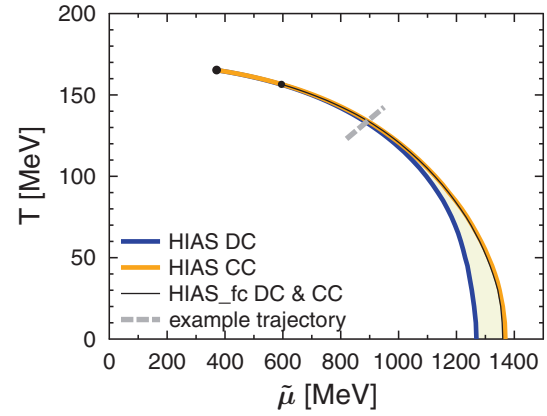

FIG. 16. (Color online) Phase diagram in the plane of temperature and Gibbs free energy per baryon $\tilde{\mu}$ for the cases of HIAS and HIAS_fc ($Y_Q = 0.3$). The thick gray line gives an example for a trajectory through the phase diagram for which we show the order parameters in Fig. 21. Otherwise, the same depiction and notation as in Fig. 15 are used. Note that the phase transition line of HIAS_fc is very close to the confinement curve (CC) of HIAS.

in Fig. 17. Here one sees that HIAS_fc is a congruent PT, because the DC and CC are identical. Furthermore, the phase transition line of HIAS_fc is inside the phase coexistence region of HIAS, as it has to be. Comparing Fig. 16 with Fig. 5 of LGAS, again one sees that the shape of the coexistence region of HIAS is much narrower. This could be described as a weaker noncongruence of the phase transition HIAS.

Note that in our calculations for HIAS we could not resolve the differences between the temperature and pressure end points and the critical point. In principle, around the critical point a similar structure as for LGAS has to occur. We predict that the phase coexistence regions of HIAS around the critical point are smooth and two-dimensional, as for LGAS in the inlays of Figs. 4–7, whereas the temperature end point and critical point could also have their orders reversed. To be more precise, we expect a rounded, "banana-shaped," region (see, e.g., Fig. 1 in Ref. [52]). However, due to the fact that for

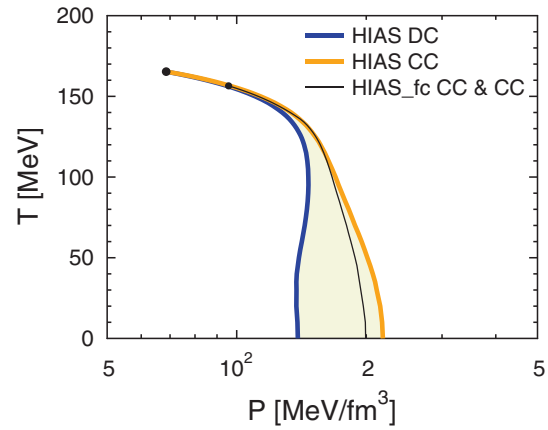

FIG. 17. (Color online) Phase diagram in the temperature-pressure plane for HIAS and HIAS_fc ($Y_Q = 0.3$). The same depiction as in Fig. 15 is used.

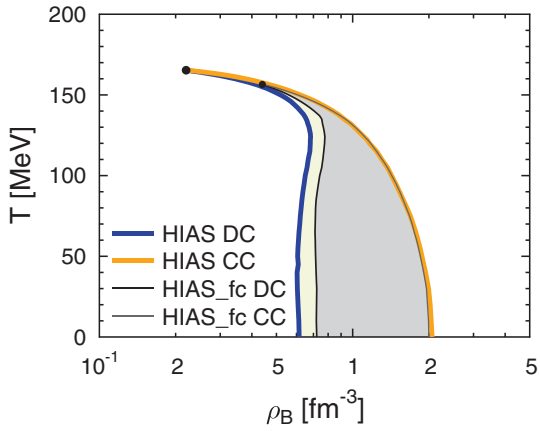

FIG. 18. (Color online) Phase diagram in the plane of temperature and baryon number density for the cases of HIAS and HIAS_fc ($Y_Q = 0.3$). Otherwise, the same depiction and notation as in Fig. 15 are used. The deconfinement curve (DC) of HIAS_fc is now to the left of the confinement curve (CC).

lower chemical potentials or baryon densities the first-order phase transitions HIS and HIAS become rather weak, i.e., the phases on both sides of the transition become extremely similar, this structure is no longer as easily observed as it is in the LGPT of nuclear matter (shown in the previous subsection) and in chemically reacting plasmas [57–62]. The highest temperature, for which we still could solve the equilibrium conditions was at $T = 165.3$ MeV for $\mu_B = 381$ MeV (respectively, $\tilde{\mu} = 371$ MeV), where we used a resolution of roughly 0.1 MeV in temperature. Because this resolution cannot be resolved on the scale of Fig. 15, we take these values of T, μ_B, and $\tilde{\mu}$ as the approximate temperature and chemical potentials of the critical point, which are also listed in Table IV. The very narrow phase coexistence region shows that the two phases are in an extremely similar thermodynamic state. For even higher temperatures, the differences between the two phases become smaller than our numerical accuracy, preventing us from finding a more precise solution.

This aspect is also very pronounced in Fig. 18, where the phase diagrams of HIAS and HIAS_fc are shown as a function of baryon number density. At $T = 0$, the DC and the CC have very different densities. Conversely, for increasing temperatures, the extension of the coexistence region in density becomes extremely narrow. Note that the coexistence region of HIAS_fc is within HIAS, as it must be.

There is one further important aspect. If we compare the phase diagram of the asymmetric system, e.g., Fig. 15, with the symmetric system in Fig. 12, and the corresponding numbers in Table IV, one finds that the critical points are practically unaffected by the change of the asymmetry. T and μ_B of HIS and HIAS differ by less than 0.5%. In the LGPT, a stronger dependence on the asymmetry is observed. For LGS and LGAS the change from $Y_Q = 0.5$ to $Y_Q = 0.3$ leads to a significant shift of the critical point, e.g., on the order of 6% in temperature. This is naturally explained by the high temperatures of order 160 MeV around the critical point of HI. The effect of the asymmetry becomes extremely weak, because the EOS in this regime is dominated by thermal contributions. Obviously, for $\mu_B \longrightarrow 0$ the EOS would be completely independent of the asymmetry. We conclude that even though HIAS is, in principle, a noncongruent PT, in our calculations with the chiral SU(3) EOS model this noncongruence is almost negligible close to the critical point. This is also visible in Figs. 15 and 16, where the width of the coexistence region is smaller than the line thickness of the curves.

Let us now come back to the explanation of the inverted ordering of DC and CC in HIAS_fc in Fig. 15. For an isothermal compression, corresponding to a horizontal line through Fig. 18, $\tilde{\mu}$ and μ_B will increase monotonically, until the deconfinement curve is reached at a certain density, $\rho_B = \rho_B^H$. This state corresponds to the value of $\mu_B = \mu_B^H$ in the hadronic phase on the deconfinement curve, i.e., the black thin line most to the right in Fig. 15. For an isothermal compression, the corresponding value of $\tilde{\mu}$ will remain constant throughout the phase transformation and $\tilde{\mu} = \tilde{\mu}^H = \tilde{\mu}^Q$. However, inside the coexistence region μ_B will change with density because it is given by

$$\mu_B = \mu_B^H \frac{\rho_B^H}{\rho_B}(1-\alpha) + \mu_B^Q \frac{\rho_B^Q}{\rho_B}\alpha, \tag{39}$$

with the volume fraction of the quark phase α (see Appendix C 1). For HIAS_fc, the hadronic phase has a higher baryon chemical potential than the quark phase, $\mu_B^H > \mu_B^Q$. Therefore, an increase of the baryon number density inside the phase coexistence region will lead to a decrease of μ_B. For $\alpha = 1$, i.e., $\rho_B = \rho_B^Q$, the CC in Fig. 15 is reached. For even higher densities μ_B will increase again.

Figures 19 and 20 show the charge fraction of each phase (hadronic and quark) as a function of the temperature and the baryon density along the phase boundaries. For clarity, we again distinguish states on the deconfinement curve by blue (dark gray) and states on the confinement curve by orange (light gray). In Figs. 19 and 20 one sees that the charge fraction in the quark phase is always less than or equal to the charge fraction in the hadronic phase. This shows that the charge fraction is also an order parameter of the QHPT. Note that

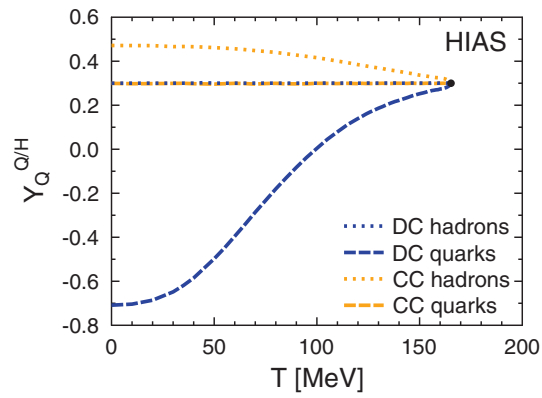

FIG. 19. (Color online) The charge fractions of the hadronic (Y_Q^H, dotted lines) and the quark phase (Y_Q^Q, dashed lines) as a function of the coexistence temperature along the phase boundary for the case of HIAS. The blue (dark gray) lines show states on the deconfinement curve DC and the orange (light gray) on the confinement curve CC.

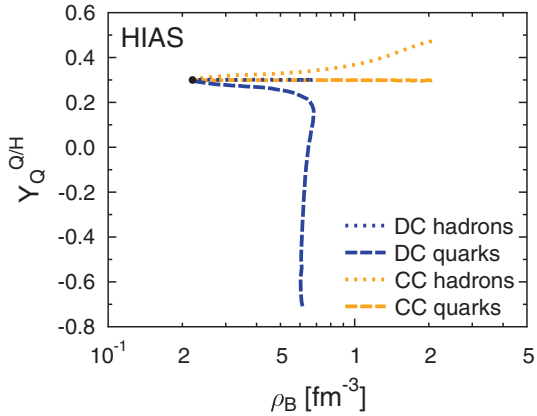

FIG. 20. (Color online) As Fig. 19 but as a function of the coexistence baryon density.

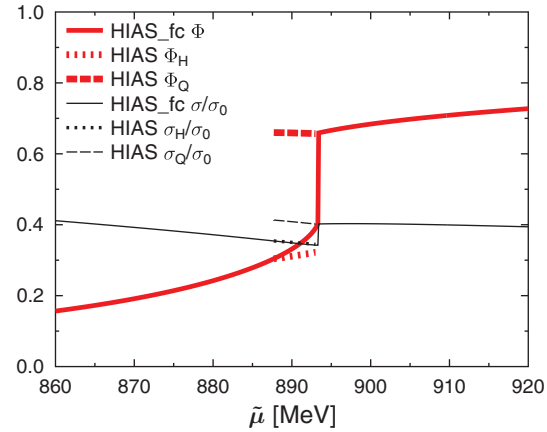

FIG. 21. (Color online) Normalized order parameter for chiral symmetry restoration/breaking σ (black thin lines) and order parameter for deconfinement/confinement Φ (red thick lines) versus the Gibbs free energy per baryon $\tilde{\mu}$ for the case of HIAS. Inside the phase coexistence region, the values of the order parameters in the quark phase (dashed lines) differ from the ones in the hadronic phase (dotted) and change during the phase transformation. HIAS_fc is the forced congruent variant, shown by solid lines. All order parameters are calculated for the trajectory through the phase diagrams shown in Fig. 16 with $T = 0.15\tilde{\mu}$.

$Y_Q^Q \leqslant Y_Q^H$ shows the opposite behavior compared to the liquid-gas PT, in which the denser phase is more symmetric.

Note also that Y_Q can, in principle, take negative values for both the hadronic and the quark phases, due to negatively charged hyperons (respectively, down and strange quarks). In the LGPT we only considered neutrons and protons, so $0 \leqslant Y_Q \leqslant 1$. For HIAS we have $-1 \leqslant Y_Q \leqslant 1$. Indeed, we observe in Fig. 19 that $Y_Q^Q < 0$ on the DC for coexistence temperatures below approximately 100 MeV. This means that the first quark matter droplets which would appear at the deconfinement phase boundary of the hadronic phase (DC) are *negatively* charged for such temperatures. Remember that on the DC only Y_Q^H is constrained to the value 0.3, and Y_Q^Q is set by the equilibrium conditions. Conversely, if the PT is crossed coming from the high density side we have $Y_Q^Q = 0.3$ on the CC. The hadronic phase on the CC shows the opposite tendency from that of quark matter. For low temperatures it approaches a rather symmetric configuration with Y_Q close to 0.5. Similar features have been discussed, e.g., in Ref. [120] for a simple quark-bag model. Figure 20 appears quite complex and differs in appearance from the equivalent Fig. 8 of LGAS. This can be explained by the nonmonotonous behavior of the density as a function of the coexistence temperature in the case of HIAS, visible in Fig. 18.

The two figures 19 and 20 also show how the charge fraction in both phases goes to 0.3 when approaching the critical point. At the critical point, the two phases are identical, i.e., have the same charge fraction, density, scalar field Φ, chiral condensate, and so on. To better understand the dynamics of such a NCPT, in Fig. 16 we included an example for a trajectory through the phase diagram for which we show the order parameters in Fig. 21. The trajectory was chosen to follow $T = 0.15\tilde{\mu}$ so the phase coexistence region is crossed at temperatures around 900 MeV and $\tilde{\mu} \sim 130$ MeV. This trajectory could, for example, be realized during the decompression of the quark-gluon plasma in a heavy-ion collision. We show the behavior of the order parameters for HIAS and HIAS_fc to illustrate the differences between a noncongruent and congruent PT. For HIAS_fc, when the phase transition line is crossed, there are jumps in σ and Φ, as expected for a first-order PT (compare also with Fig. 11). The quark phase is characterized by having a larger value of Φ, showing that it represents the deconfined state. As can be seen from Eqs. (5) and (6), this increases the effective mass of baryons but decreases the effective mass of quarks. Note that σ, which is decreasing with increasing $\tilde{\mu}$ in both of the two phases, locally increases at the PT (going from left to right), because the value of σ is higher in the quark phase. This is in contrast to the typical expectation of other models, which give partial chiral symmetry restoration, i.e., a lower value of σ in the quark phase. This effect found in our calculations comes from the fact that in the chiral SU(3) model both order parameters σ and Φ are connected through the effective masses of the particles. Also the baryonic density of the quarks (not counting the contribution from U) is less than the one of the hadrons. This leads to a decrease of the scalar field across the phase transition.

In Fig. 21 it can be seen that in the noncongruent phase transition HIAS the behavior of the order parameters is more complex. Within the phase coexistence region, i.e., within the DC and CC shown in Fig. 16, the hadronic and the quark phases are in coexistence. The two phases are spatially separated and in each of the two phases one has different values of the order parameters. At the onset of the PT at the confinement curve one has $\alpha = 1$, i.e., the volume fraction of the quark phase is still 1 and the volume fraction of the hadronic phase is 0. Inside the phase coexistence region, the quark phase has a larger value of Φ but also a slightly increased chiral condensate σ, as observed for HIAS_fc before. With decreasing $\tilde{\mu}$, not only the volume fraction of the quark phase decreases, but also the properties of the two phases change. One clearly sees that chiral symmetry breaking proceeds in both of the two phases with decreasing density. On the other hand, Φ^H is decreasing, and Φ^Q is slightly increasing. When the deconfinement curve is reached, $\alpha = 0$ and only the hadronic phase is left. After this

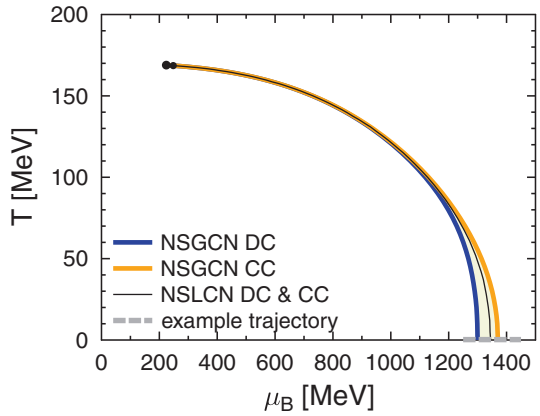

FIG. 22. (Color online) Phase diagram in the temperature-baryon chemical potential plane for neutron stars with local (NSLCN) and global charge neutrality (NSGCN). The horizontal thick gray line at $T = 0$ is a trajectory through the phase diagram, for which we show the order parameters in Fig. 23. The large black dot is the critical point of NSGCN, and the small one the pseudocritical point of NSLCN.

in Fig. 21 one sees that Φ^H and σ^H become equal to values obtained for HIAS_fc.

Finally, we discuss results for the quark-hadron phase transition in neutron stars shown in Fig. 22. Let us reiterate that in this paper we consider the quark-hadron PT in multicomponent matter of neutron stars of macroscopic coexisting phases (i) with local charge neutrality and (ii) in the variant of global charge neutrality within the Coulombless approximation. It is just the Coulombless approximation which justifies the use of Gibbs conditions instead of Gibbs-Guggenheim conditions, which are valid for true macroscopic Coulomb systems (e.g., Ref. [52]). Local and global charge neutrality constraints lead to forced-congruent ("Maxwell") and noncongruent ("Gibbs") PTs. As discussed in Sec. II B, the choice between local or global charge neutrality can be associated with the unknown surface tension between the two phases.

The phase diagram of neutron stars looks similar to the one shown in Fig. 16. In contrast, the dimensionality of HIAS_fc in Fig. 15 differs from the one of NSLCN in Fig. 22. This is easy to understand, because $\mu_B^Q = \mu_B^H$ is valid for NSLCN and NSGCN and for HIAS but not for HIAS_fc. The critical points of the neutron star cases are at lower μ_B and slightly higher T than in the cases of HIAS and HIS, i.e., the phase transition regions extend to higher temperatures. Asymmetry and charge neutrality do not seem to have a major effect at such high temperatures. Therefore, we relate this difference to the treatment of strangeness (see Table III). At $T = 0$ the width of the phase coexistence region of HIAS is 52 MeV, and for NSGCN it is 70.2 MeV. With the chiral SU(3) model used here, the hadron-quark PT and the noncongruent features at $T = 0$ seem to be stronger for neutron star matter than for matter in heavy-ion collisions. This is a result of the larger asymmetries obtained in β equilibrium due to the large degeneracy of electrons and also because of the different constraints used for strangeness.

The critical point of NSGCN is at approximately $T^{\rm CP} = 168.9$ MeV and $\mu_B^{\rm CP} = 224$ MeV, and that of NSLCN is at $T^{\rm CP} = 168.6$ MeV and $\mu_B^{\rm CP} = 247$ MeV (see also Table IV). Interestingly, they differ only slightly. It shows that the treatment of electric charge neutrality plays only a minor role for the location of critical points of the QHPT at the typical high temperatures. The local constraint applied in HIAS_fc which does not allow isospin diffusion has a slightly larger effect at high temperatures.

The phase transition line for NSLCN with enforced local charge neutrality must lie strictly within the phase coexistence region of NSGCN, in accordance with general rules for NCPTs (e.g., Refs. [57–62]). Both boundaries can touch each other in points of azeotropic composition. Here this would mean that the two phases were charge neutral *a priori*. Actually, this is not the case, but they only touch because of the thickness of the lines in the figure. For NSLCN, μ_Q will not behave continuously when the phase transition line is crossed, as already discussed at the end of Sec. V C, because μ_Q^H differs from μ_Q^Q. This is in accordance with general properties of phase coexistence of charge neutral, macroscopic phases in Coulomb systems (see, e.g., Refs. [52,61,121,122]): Any phase-interface in macroscopic equilibrium Coulomb systems is accompanied by a finite difference in the average electrostatic potentials of both coexisting phases (Galvani potential), see also Sec. II B and compare also with Ref. [123]. However, the total charge chemical potential μ_Q still can be related to the local chemical potentials μ_Q^H and μ_Q^Q if it is seen as a function of baryon number density. Based on two different assumptions about the implementation of local charge neutrality, in Appendix C 3 we derive the following expressions:

$$\mu_Q = \begin{cases} (1-\alpha)\mu_Q^H + \alpha\mu_Q^Q, & \text{for} \quad \rho_Q^H \equiv \rho_Q^Q \\ (1-\alpha)\frac{\rho_B^H}{\rho_B}\mu_Q^H + \alpha\frac{\rho_B^Q}{\rho_B}\mu_Q^Q, & \text{for} \quad Y_Q^H \equiv Y_Q^Q. \end{cases} \tag{40}$$

It would be more intuitive to assume the first of the two conditions. These expressions can be used to determine the total chemical potential of charged particles inside the two-phase mixture.

Figure 22 also includes an example trajectory through the phase transition region at $T = 0$. This trajectory could correspond, for example, to the spatial structure inside a

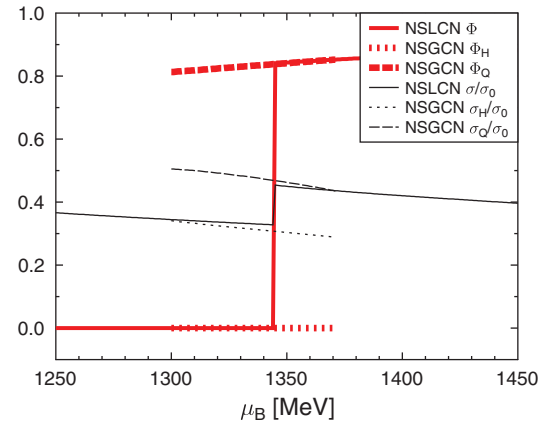

FIG. 23. (Color online) As shown in Fig. 21 but for the cases of NSLCN and NSGCN of the example trajectory at $T = 0$.

neutron star, or better called a hybrid star. In Fig. 23 we show the behavior of the order parameters for the cases of NSLCN and NSGCN along the trajectory. For $T = 0$, we find $\Phi^H = 0$, i.e., the hadronic phase is completely confined. For finite temperatures this is not the case, as can be seen in Figs. 11 and 21, where one has some sequential deconfinement already in the hadronic phase. Otherwise, similar features are observed as in Fig. 21. The obtained jumps show that we have a first-order PT. The different values of the order parameters distinguish the two spatially separated phases. If the PT is noncongruent, one obtains a phase coexistence region, and the phases change their properties, including the order parameters, during the phase transformation.

VII. SUMMARY AND CONCLUSIONS

In this article we investigated the liquid-gas phase transition (LGPT) described by the FSUgold relativistic mean-field model and the quark-hadron (QH) or deconfinement phase transition with the chiral SU(3) model. We did not take into account any explicit Coulomb interactions or other finite-size effects but always considered phase coexistence of macroscopic phases. Different physical systems were investigated: heavy-ion collisions of symmetric nuclei at low (LGS) and high collision energies (HIS) and of asymmetric nuclei with $Z/A = 0.3$ at low (LGAS) and high collision energies (HIAS). Furthermore, we also studied the QHPT in NS. The main goal of our work is to characterize the first-order phase transitions in the different systems regarding their possible noncongruence and to identify the typical noncongruent aspects. This characterization and classification, and our qualitative results, should not depend on the model used for the calculations but should be valid in a rather general way. In our study of noncongruent phase transitions we used essential features of such types of phase transitions obtained from terrestrial applications with high-temperature chemically reacting plasmas [57–62].

A noncongruent, first-order phase transition occurs for a nonunary system with more than one (globally) conserved charge where the charge ratios change during a phase transformation. In principle, all the investigated scenarios contain several conserved charges, with at least baryon number and electric charge. However, due to isospin symmetry, for the symmetric case (LGS and HIS), matter always stays symmetric, even if there is phase coexistence, which is called "azeotropic" behavior. Only these two cases lead to congruent phase transitions. To further illustrate the differences between a congruent and a noncongruent phase transition, we also considered the cases of LGAS_fc and HIAS_fc, where we forced the system to have a congruent phase transition, by constraining the local charge fractions to be equal in the two phases. From a physical point of view, the forced-congruent treatment of phase transformations is not completely artificial but corresponds to the so-called frozen diffusion approximation. In a similar way we considered enforced local charge neutrality in neutron stars in the case of NSLCN instead of global charge neutrality (NSGCN). In Table V we summarize the classification of the phase transitions in the different physical systems.

TABLE V. Classification of the equilibrium conditions and type of first-order phase transition in the different scenarios.

Case	Equilibrium conditions	Type of PT
LGS	Gibbs/Maxwell (equiv.)	Congruent (azeotrope)
LGAS	Gibbs	Noncongruent
LGAS_fc	Maxwell	Forced congruent
HIS	Gibbs/Maxwell (equiv.)	Congruent (azeotrope)
HIAS	Gibbs	Noncongruent
HIAS_fc	Maxwell	Forced congruent
NSLCN	Maxwell	Forced congruent
NSGCN	Gibbs	Noncongruent

In the astrophysics community, congruent and noncongruent phase transitions are usually called "Maxwell" and "Gibbs" phase transitions, referring to the way in which phase coexistence is calculated. Because of the constant charge ratios and the fact that all properties of the two phases do not change for an isothermal phase transformation, a simple Maxwell construction can be used for the congruent case. Conversely, for noncongruent phase transitions, the more complicated Gibbs construction is necessary to solve the set of thermal, mechanical, and multiple chemical equilibrium conditions. Due to their prominent role in neutron star physics, NSLCN and NSGCN are considered the two most representative scenarios. However, as we demonstrated, they are only examples illustrating the further classification of first-order phase transitions to be either congruent or noncongruent.

The distinction between congruent and noncongruent phase transitions is crucial for the dimensionality of phase diagrams. For a given temperature T, a congruent phase transition occurs at a single value of the Gibbs free energy per baryon $\tilde{\mu}$. Therefore, in the T-$\tilde{\mu}$ plane, one obtains a phase transition line, as well as in the T-P and P-$\tilde{\mu}$ planes, and generally in any pair of intensive thermodynamic variables [52]. Conversely, for a noncongruent phase transition calculated with the Gibbs construction and a given chemical composition, in any pair of intensive thermodynamic variables one obtains two-dimensional "banana-like" phase-coexistence regions (see, e.g., Fig. 1 in Ref. [52]). One of the conclusions from the present study is that all asymmetric systems are noncongruent if no additional local constraints are enforced. The corresponding phase diagrams should always be regions and not lines.

Inside the phase coexistence region, the order parameters (e.g., density and charge fraction for LG, density, charge fraction, chiral condensate, and Φ field representing the Polyakov-loop for QHPT) have different values in the two phases, which is the actual definition of a first-order phase transition. We demonstrated the behavior of some of these order parameters on the binodal boundaries and within two-phase regions and how they become equal at the critical point. Furthermore, for the QHPT this was also illustrated for the chiral condensate and the Φ field for trajectories through the phase diagram in a high-energy heavy-ion collision and in a neutron star. For a congruent phase transition, the different values appear as a jump when crossing the phase transition line and moving from one phase to the other.

For noncongruent phase transitions, at the phase coexistence boundary the second phase appears, and its volume fraction increases until the first phase has disappeared completely when the phase coexistence region has been crossed. During such a noncongruent phase transformation, both phases continuously change their thermodynamic properties and order parameters.

Local charge neutrality for macroscopic phase coexistence in neutron stars under Maxwell conditions has been applied in a number of published works. It is well known that the local charge chemical potentials behave discontinuously in such a transition, while the generalized nonlocal electrochemical potentials are continuous in accordance with generalized Gibbs-Guggenheim conditions (e.g., Ref. [52]). The discontinuity is associated with the so-called Galvani potential of the phase interface in Coulomb systems (e.g., Refs. [61] and [124]). In the present article, for the Coulombless approximation we derived expressions for the total charge chemical potential μ^Q inside the phase coexistence region as a function of the total baryon number density, which behaves continuously. The new expressions show explicitly that the total chemical potentials on the binodal surface correspond to the ones of the dominating phase if its volume fraction is unity. We also derived the total chemical potentials for the other phase transitions where local constraints were applied.

Another fundamental aspect of noncongruent phase transitions is the location and properties of the critical point. For congruent phase transitions, the critical point is located at the end of the phase transition line. Conversely, the phase coexistence region of a noncongruent phase transition has several (topological) end points, namely for temperature, pressure, and chemical potential, which all differ (e.g., Ref. [52]). The critical point, as the point of thermodynamic singularity, and where the two phases are identical, does not coincide with these end points. For the LGPT we found that the temperature end point is located on the saturation curve, i.e., the critical point is located at higher densities than the temperature end point, while the pressure end point is located on the boiling curve. This is the same arrangement as for noncongruent phase transitions in terrestrial chemically reacting plasma (e.g., Fig. 1 in Ref. [52]). The properties of all (pseudo-) critical points found in the present study are listed in Table IV.

For the QHPT we could not resolve the end points and the critical points because we reached the limit of our numerical accuracy. But, at the same time, this is related to another important finding from our study: at low temperatures, the asymmetry has a significant impact on the phase diagrams of the QHPT. Conversely, for high temperatures, close to the critical point, this impact is vanishingly small because the EOS is dominated by thermal contributions. As a consequence, the noncongruent features of HIAS are almost unnoticable close to the critical point. This is in contrast to LGAS of nuclear matter considered here and the LGPT in terrestrial chemically reacting plasma [57–62] for which the noncongruence is significant for all conditions.

Another important difference between the LGPT and QHPT comes from the phase diagrams in the temperature-pressure plane. For ordinary Van-der-Waals-like phase transitions of liquid-gas type, and also for the numerous variants of the LGPT in nucleonic matter studied in other papers, the slope of the P-T phase transition line is positive, which we also confirm in our study. Conversely, for the QHPT, we found that the slope is negative, which leads to the conclusion that this phase transition is not of liquid-gas type. The Clapeyron equation shows that this peculiar feature is a result of the generally higher entropy per baryon of the quark phase than of the hadronic phase during phase coexistence. We also found that the denser phase of the QHPT (the quark phase) is more asymmetric than the more dilute phase (the hadronic phase), which is also opposite the behavior in the LGPT.

In the future, we could extend our work to study phase diagrams of protoneutron stars and supernovae. Those objects are special, not only for having higher temperature in comparison to neutron stars but also for having a higher fixed lepton content due to the presence of trapped neutrinos. Such features transform an already binary phase transition into a ternary one due to the introduction of the lepton number conservation, with potentially interesting results. It was already shown that a phase transition to deconfined matter prior to the supernova explosion can have observable effects [125]. Another aspect which we did not discuss in detail are the consequences of different constraints regarding strangeness conservation and possible strangeness distillation.

It would be interesting to explore further the experimental consequences of noncongruence in heavy-ion collisions. In our investigations we have found that the noncongruence of the QHPT increases with decreasing temperature. Therefore, the possible noncongruent features could become particularly relevant for the heavy-ion experiments at the future FAIR facility at Darmstadt or NICA at Dubna, which both aim to probe asymmetric matter at high densities and low temperatures.

ACKNOWLEDGMENTS

The authors thank Michael Strickland for proofreading the manuscript. I.I. acknowledges also V. Fortov, D. Blaschke, and J. Randrup for support and fruitful discussions. M.H. acknowledges support from the High Performance and High Productivity Computing (HP2C) project and the Swiss National Science Foundation (SNF) under Grant No. 200020-132816/1. This work has been supported additionally by CompStar, a research networking program of the European Science Foundation. M.H. is also grateful for participating in the EuroGENESIS collaborative research program of the ESF and the ENSAR/THEXO project. I.I. acknowledges support from the Scientific Program "Physics of extreme states of matter" of the Russian Academy of Science and Education Center and "Physics of high energy density matter" of the Moscow Institute of Physics and Technology. The work of I.I. was also partially supported by the Extreme Matter Institute (EMMI, Germany).

APPENDIX A: CRITICAL POINTS IN A "TWO-EOS" DESCRIPTION

It is well known (e.g., Ref. [53]) that in a "two-EOS" description of PTs, where two different EOS models are used for the two phases in coexistence, there cannot be a termination

point or critical point of a phase transition line. This is due to the standard argument of the impossibility of a continuous and smooth transformation from one phase into another in a two-EOS approach (e.g., commonly used for crystal-fluid coexistence). This is in contrast to the claims in the recent studies of, e.g., Refs. [38,126–128]. The previous statement can be supported with the following geometrical argumentation. For symmetric matter, the two phases give two different planes in the parameter space of pressure P, temperature T, and baryon chemical potential μ_B. Where the two planes intersect, one has phase coexistence. This intersection of two two-dimensional planes in a three-dimensional parameter space either has to be a closed or an infinite curve. A termination point of the intersection curve is impossible, as long as the planes do not show any discontinuities, which would be rather unphysical. This argumentation can also be generalized to asymmetric matter, where the charge chemical potential μ_Q appears as another dimension.

APPENDIX B: AZEOTROPIC BEHAVIOR FOR SYMMETRIC MATTER IN HIS AND LGS

The azeotropic behavior of HIS and LGS can be explained as a result of isospin symmetry in the following way. First, it is important to note that from $Y_Q = 0.5$ it follows that the total third component of the isospin is zero, $I_3 = 0$, if there is no net strangeness, $S = 0$. Furthermore, the considered particles (neutrons and protons for LGS; u, d, s quarks, and the baryon octet for HIS) can be grouped in pairs of isospin partners, where the isospin partners have identical baryon number, strangeness, and mass, but opposite third component of the isospin, and some remaining particles with a zero third component of the isospin. If, in addition, the interactions are built in an isospin-symmetric way, namely that they are identical for the isospin partners at $I_3 = 0$, it follows that $I_3 = 0$ if and only if the isospin chemical potential is also zero, $\mu_{I_3} = \frac{\partial F}{\partial I_3} = 0$. For the constraints used in LGS and HIS, all these conditions are fulfilled by the two applied EOS models FSUgold and chiral SU(3). On the other hand, it can be shown that the charge chemical potential is equal to the isospin chemical potential, $\mu_{I_3} = \mu_Q$. Thus, we obtain that $\mu_Q = 0$ if $Y_Q = 0.5$ and $S = 0$ but independent of temperature and density. For two-phase coexistence in HIS and LGS we use the constraints $S^{\mathrm{I}} = S^{\mathrm{II}} = 0$ and $Y_Q = 0.5$. Therefore, we get $\mu_Q^{\mathrm{I}} = \mu_Q^{\mathrm{II}} = 0$ and $Y_Q^{\mathrm{I}} = Y_Q^{\mathrm{II}} = 0.5$, which shows that the two phases remain symmetric and that the PT is, therefore, azeotropic.

APPENDIX C: TOTAL CHEMICAL POTENTIALS INSIDE THE PHASE-COEXISTENCE REGIONS

In all cases of HI and LG local constraints are applied for two-phase coexistence. Therefore, it is necessary to refine the definition of the total chemical potentials inside the two-phase mixture and to relate them to the local chemical potentials already defined in Table II.

1. HIAS_fc and LGAS_fc

Let us start with the cases of LGAS_fc and HIAS_fc. The constraints listed in Table III are equivalent to considering $B = \text{const.}$, $Q = \text{const.} = Y_Q B$, $Y_Q^{\mathrm{I}} = Y_Q^{\mathrm{II}}$, and $S^{\mathrm{I}} = S^{\mathrm{II}} = 0$. Note that this set of constraints also gives $Y_Q = Y_Q^{\mathrm{I}} = Y_Q^{\mathrm{II}}$. The constraint for zero local strangeness, $S^{\mathrm{I}} = S^{\mathrm{II}} = 0$, is formulated with local extensive variables. However, it would be equivalent to consider $Y_S^{\mathrm{I}} = Y_S^{\mathrm{II}}$ and $S = 0$, or $\rho_S^{\mathrm{I}} = \rho_S^{\mathrm{II}}$ and $S = 0$, where we define $Y_S^{\mathrm{I}} = S^{\mathrm{I}}/B^{\mathrm{I}}$, $\rho_S^{\mathrm{I}} = S^{\mathrm{I}}/V^{\mathrm{I}}$, and analogous expressions for phase II. In conclusion, we have the simple conservation of the total charges, which are fixed to some values, plus two additional local constraints $Y_Q^{\mathrm{I}} = Y_Q^{\mathrm{II}}$ and $Y_S^{\mathrm{I}} = Y_S^{\mathrm{II}}$, or $Y_Q^{\mathrm{I}} = Y_Q^{\mathrm{II}}$ and $\rho_S^{\mathrm{I}} = \rho_S^{\mathrm{II}}$. Let us, first, use the first of the two formulations of the two local constraints.

Now we can define the total baryon chemical potential inside the two-phase mixture as the following derivative:

$$\mu_B = \left.\frac{\partial F}{\partial B}\right|_{T,V,S,Q,Y_Q^{\mathrm{I}}=Y_Q^{\mathrm{II}},Y_S^{\mathrm{I}}=Y_S^{\mathrm{II}}}. \tag{C1}$$

This is nothing but the definition of μ_B outside the two-phase mixture given in Table I but with the additional local constraints taken into account. This is what we mean by the total chemical potentials inside the two-phase mixtures. For the definition of μ_Q, "Q" and "B" have to be exchanged in Eq. (C1) and for μ_S it is "S" and "B". For $\tilde{\mu}$, only "Q" has to be replaced by "Y_Q" in the list of constant variables. Note that this definition of $\tilde{\mu}$ gives the same relation,

$$\tilde{\mu} = Y_Q \mu_Q + \mu_B, \tag{C2}$$

obtained previously for single phases. Let us introduce $\mathbf{X}$ as an abbreviation for the set of variables kept constant and the local constraints,

$$\mu_B = \left.\frac{\partial F}{\partial B}\right|_{\mathbf{X}}. \tag{C3}$$

For the definition of the total chemical potentials of other cases than HIAS_fc and LGAS_fc, one only has to exchange the local constraints in $\mathbf{X}$.

Now we want to evaluate the above expression for μ_B in HIAS_fc and LGAS_fc. Inside the two-phase mixture, the total free energy F is given as the sum of the two phases

$$F = F^{\mathrm{I}}(T, V^{\mathrm{I}}, B^{\mathrm{I}}, S^{\mathrm{I}}, Q^{I}) + F^{\mathrm{II}}(T, V^{\mathrm{II}}, B^{\mathrm{II}}, S^{\mathrm{II}}, Q^{\mathrm{II}}), \tag{C4}$$

where we used thermal equilibrium, Eq. (15). With the chain rule and the definitions of the local chemical potentials of Table II we obtain

$$\begin{aligned}\mu_B = &-\left.\frac{\partial V^{\mathrm{I}}}{\partial B}\right|_{\mathbf{X}} P^{\mathrm{I}} - \left.\frac{\partial V^{\mathrm{II}}}{\partial B}\right|_{\mathbf{X}} P^{\mathrm{II}} + \left.\frac{\partial B^{\mathrm{I}}}{\partial B}\right|_{\mathbf{X}} \mu_B^{\mathrm{I}} \\ &+ \left.\frac{\partial B^{\mathrm{II}}}{\partial B}\right|_{\mathbf{X}} \mu_B^{\mathrm{II}} + \left.\frac{\partial S^{\mathrm{I}}}{\partial B}\right|_{\mathbf{X}} \mu_S^{\mathrm{I}} + \left.\frac{\partial S^{\mathrm{II}}}{\partial B}\right|_{\mathbf{X}} \mu_S^{\mathrm{II}} \\ &+ \left.\frac{\partial Q^{\mathrm{I}}}{\partial B}\right|_{\mathbf{X}} \mu_Q^{\mathrm{I}} + \left.\frac{\partial Q^{\mathrm{II}}}{\partial B}\right|_{\mathbf{X}} \mu_Q^{\mathrm{II}}.\end{aligned} \tag{C5}$$

Because of pressure equilibrium, Eq. (14), the first two terms sum up to zero. Next we use $S^{\mathrm{I}} = Y_S^{\mathrm{I}} B^{\mathrm{I}}$ for the expression

$\frac{\partial S^{\rm I}}{\partial B}|_{\mathbf{X}}$,

$$\left.\frac{\partial S^{\rm I}}{\partial B}\right|_{\mathbf{X}} = Y_S^{\rm I}\left.\frac{\partial B^{\rm I}}{\partial B}\right|_{\mathbf{X}} + B^{\rm I}\left.\frac{\partial Y_S^{\rm I}}{\partial B}\right|_{\mathbf{X}} = B^{\rm I}\left.\frac{\partial Y_S^{\rm I}}{\partial B}\right|_{\mathbf{X}}, \tag{C6}$$

where the second equality comes from $Y_S^{\rm I} = 0$. If we have $Y_S^{\rm I} = Y_S^{\rm II}$, we also have $Y_S^{\rm I} = Y_S^{\rm II} = Y_S$ and, thus,

$$B^{\rm I}\left.\frac{\partial Y_S^{\rm I}}{\partial B}\right|_{\mathbf{X}} = B^{\rm I}\left.\frac{\partial Y_S}{\partial B}\right|_{\mathbf{X}} = -\frac{B^{\rm I}}{B}Y_S = 0. \tag{C7}$$

In conclusion, we obtain $\frac{\partial S^{\rm I}}{\partial B}|_{\mathbf{X}} = 0$, and, in the same way, $\frac{\partial S^{\rm II}}{\partial B}|_{\mathbf{X}} = 0$. Thus, we are left with

$$\begin{aligned}\mu_B = &\left.\frac{\partial B^{\rm I}}{\partial B}\right|_{\mathbf{X}}\mu_B^{\rm I} + \left.\frac{\partial B^{\rm II}}{\partial B}\right|_{\mathbf{X}}\mu_B^{\rm II} \\ &+ \left.\frac{\partial Q^{\rm I}}{\partial B}\right|_{\mathbf{X}}\mu_Q^{\rm I} + \left.\frac{\partial Q^{\rm II}}{\partial B}\right|_{\mathbf{X}}\mu_Q^{\rm II}.\end{aligned} \tag{C8}$$

To make use of the local constraint $Y_Q^{\rm I} = Y_Q^{\rm II}$ in $\mathbf{X}$, we replace $Q^{\rm I}$ with $Y_Q^{\rm I}B^{\rm I}$ and $Q^{\rm II}$ with $Y_Q^{\rm II}B^{\rm II}$ and use $Y_Q = Y_Q^{\rm I} = Y_Q^{\rm II}$. This gives

$$\begin{aligned}\mu_B = &\left.\frac{\partial B^{\rm I}}{\partial B}\right|_{\mathbf{X}}\left(\mu_B^{\rm I} + Y_Q^{\rm I}\mu_Q^{\rm I}\right) + \left.\frac{\partial B^{\rm II}}{\partial B}\right|_{\mathbf{X}}\left(\mu_B^{\rm II} + Y_Q^{\rm II}\mu_Q^{\rm II}\right) \\ &- \frac{B^{\rm I}}{B}Y_Q^{\rm I}\mu_Q^{\rm I} - \frac{B^{\rm II}}{B}Y_Q^{\rm II}\mu_Q^{\rm II}.\end{aligned} \tag{C9}$$

Now we can use the interphase equilibrium conditions (31) and (32), and the definitions of $\tilde{\mu}^{\rm I}$ and $\tilde{\mu}^{\rm II}$ [Eq. (34)], to obtain

$$\begin{aligned}\mu_B = &\ \tilde{\mu}^{\rm I} - \frac{B^{\rm I}}{B}Y_Q^{\rm I}\mu_Q^{\rm I} - \frac{B^{\rm II}}{B}Y_Q^{\rm II}\mu_Q^{\rm II}, \\ = &\ \frac{B^{\rm I}}{B}\tilde{\mu}^{\rm I} + \frac{B^{\rm II}}{B}\tilde{\mu}^{\rm II} - \frac{B^{\rm I}}{B}Y_Q^{\rm I}\mu_Q^{\rm I} - \frac{B^{\rm II}}{B}Y_Q^{\rm II}\mu_Q^{\rm II}, \\ = &\ \frac{B^{\rm I}}{B}\mu_B^{\rm I} + \frac{B^{\rm II}}{B}\mu_B^{\rm II}.\end{aligned} \tag{C10}$$

This can be written as

$$\mu_B = (1-\alpha)\frac{\rho_B^{\rm I}}{\rho_B}\mu_B^{\rm I} + \alpha\frac{\rho_B^{\rm II}}{\rho_B}\mu_B^{\rm II}, \tag{C11}$$

where α is the volume fraction of phase II in the two-phase mixture,

$$\alpha = \frac{\rho_B - \rho_B^{\rm I}}{\rho_B^{\rm II} - \rho_B^{\rm I}}. \tag{C12}$$

For $\rho_B = \rho_B^{\rm I}$, one gets $\mu_B = \mu_B^{\rm I}$, and, for $\rho_B = \rho_B^{\rm II}$, $\mu_B = \mu_B^{\rm II}$, i.e., the correct limits are obtained. Furthermore, if $\mu_B^{\rm I} = \mu_B^{\rm II}$, one finds that $\mu_B = \mu_B^{\rm I} = \mu_B^{\rm II}$, independent of ρ_B. With a similar derivation, one obtains the following expression for the total charge chemical potential:

$$\mu_Q = (1-\alpha)\frac{\rho_B^{\rm I}}{\rho_B}\mu_Q^{\rm I} + \alpha\frac{\rho_B^{\rm II}}{\rho_B}\mu_Q^{\rm II}. \tag{C13}$$

It turns out that one obtains the same expressions (C11) and (C13) if one uses the strangeness constraint in the form $\rho_S^{\rm I} = \rho_S^{\rm II}$ instead of $Y_S^{\rm I} = Y_S^{\rm II}$. Furthermore, note that Eqs. (C11), (C13), and (C2) also allow one to express $\tilde{\mu}$ in terms of the local chemical potentials.

Interestingly, for the total strange chemical potential the form of the strangeness constraint makes a difference,

$$\mu_S = \begin{cases}(1-\alpha)\mu_S^{\rm I} + \alpha\mu_S^{\rm II}, & \text{for} \quad \rho_S^{\rm I} = \rho_S^{\rm II} \\ (1-\alpha)\frac{\rho_B^{\rm I}}{\rho_B}\mu_S^{\rm I} + \alpha\frac{\rho_B^{\rm II}}{\rho_B}\mu_S^{\rm II}, & \text{for} \quad Y_S^{\rm I} = Y_S^{\rm II}.\end{cases} \tag{C14}$$

Note that the two forms give identical results if $\alpha = 0$ or if $\alpha = 1$, i.e., at the phase boundaries.

Equations (C11), (C13), and (C14) can be used to determine the chemical potential of particles for the two-phase mixture as a whole. For example, for protons and neutrons, one obtains, using Eq. (10),

$$\mu_p = (1-\alpha)\frac{\rho_B^{\rm I}}{\rho_B}\mu_p^{\rm I} + \alpha\frac{\rho_B^{\rm II}}{\rho_B}\mu_p^{\rm II}, \tag{C15}$$

$$\mu_n = (1-\alpha)\frac{\rho_B^{\rm I}}{\rho_B}\mu_n^{\rm I} + \alpha\frac{\rho_B^{\rm II}}{\rho_B}\mu_n^{\rm II}. \tag{C16}$$

For Λ's the constraint $Y_S^{\rm I} = Y_S^{\rm II}$ would, for example, lead to

$$\mu_\Lambda = (1-\alpha)\frac{\rho_B^{\rm I}}{\rho_B}\mu_\Lambda^{\rm I} + \alpha\frac{\rho_B^{\rm II}}{\rho_B}\mu_\Lambda^{\rm II}. \tag{C17}$$

2. LGS, LGAS, HIS, and HIAS

In the cases of LGS, LGAS, HIS, and HIAS, the only local constraint is $S^{\rm I} = S^{\rm II} = 0$. Here one finds

$$\mu_B = \mu_B^{\rm I} = \mu_B^{\rm II}, \tag{C18}$$

$$\mu_Q = \mu_Q^{\rm I} = \mu_Q^{\rm II}, \tag{C19}$$

$$\mu_S = \begin{cases}(1-\alpha)\mu_S^{\rm I} + \alpha\mu_S^{\rm II}, & \text{for} \quad \rho_S^{\rm I} = \rho_S^{\rm II} \\ (1-\alpha)\frac{\rho_B^{\rm I}}{\rho_B}\mu_S^{\rm I} + \alpha\frac{\rho_B^{\rm II}}{\rho_B}\mu_S^{\rm II}, & \text{for} \quad Y_S^{\rm I} = Y_S^{\rm II}.\end{cases} \tag{C20}$$

3. NSLCN and NSGCN

For the case of NSGCN, which uses the Coulombless approximation and leads to a noncongruent PT, all three local chemical potentials have equal values in the two phases and one obtains

$$\mu_B = \mu_B^{\rm I} = \mu_B^{\rm II}, \tag{C21}$$

$$\mu_Q = \mu_Q^{\rm I} = \mu_Q^{\rm II}, \tag{C22}$$

$$\mu_S = \mu_S^{\rm I} = \mu_S^{\rm II}(= 0). \tag{C23}$$

In Table III, the local charge neutrality constraint in NSLCN was formulated as $Y_Q^{\rm I} = Y_Q^{\rm II} = 0$, i.e., in terms of the local electric charge fractions. Here one has a similar situation as for the local strangeness constraint in Appendix C 1: It would be equivalent to consider $\rho_Q^{\rm I} = \rho_Q^{\rm II} = 0$ instead of $Y_Q^{\rm I} = Y_Q^{\rm II} = 0$. After a similar derivation as in Appendix C 1 one obtains

$$\mu_B = \mu_B^{\rm I} = \mu_B^{\rm II}, \tag{C24}$$

$$\mu_S = \mu_S^{\rm I} = \mu_S^{\rm II}(= 0), \tag{C25}$$

$$\mu_Q = \begin{cases}(1-\alpha)\mu_Q^{\rm I} + \alpha\mu_Q^{\rm II}, & \text{for} \quad \rho_Q^{\rm I} = \rho_Q^{\rm II} \\ (1-\alpha)\frac{\rho_B^{\rm I}}{\rho_B}\mu_Q^{\rm I} + \alpha\frac{\rho_B^{\rm II}}{\rho_B}\mu_Q^{\rm II}, & \text{for} \quad Y_Q^{\rm I} = Y_Q^{\rm II}.\end{cases} \tag{C26}$$

For the determination of μ_Q it makes a difference whether one assumes equal charge fractions or equal charge densities in the two phases. It would be more intuitive to assume the first of the two conditions, namely that additional charge is distributed uniformly, because here we have in mind that the Coulomb forces are the reason for local charge neutrality.

APPENDIX D: GIBBS FREE ENERGY

Let us, first, assume we are outside of the two-phase coexistence region, i.e., there is only one phase. The Gibbs free energy G can be obtained via a Legendre transformation from the (Helmholtz) free energy F,

$$G = F + PV. \tag{D1}$$

If $G = G(T, P, \{N_i\})$ is seen as a function of the particle numbers N_i, which are fixed by Eq. (10), one obtains

$$G = \sum_i N_i \mu_i, \tag{D2}$$

$$= B\mu_B + Q\mu_Q + S\mu_S. \tag{D3}$$

This shows that G can also be seen as a function of B, Q, and S, i.e., $G = (T, P, B, Q, S)$. Furthermore, because we consider either $S = 0$ or $\mu_S = 0$, we obtain from Eqs. (D3), (7), and (8),

$$G = B\mu_B + Q\mu_Q, \tag{D4}$$

$$= B\tilde{\mu}, \tag{D5}$$

which shows that $\tilde{\mu}$ is indeed the Gibbs free energy per baryon (respectively, the two definitions are equivalent).

Inside the two-phase mixture we have

$$G = G\big(T, P, \{N_i^{\mathrm{I}}\}, \{N_i^{\mathrm{II}}\}\big)$$

$$= G^{\mathrm{I}}\big(T, P, \{N_i^{\mathrm{I}}\}\big) + G^{\mathrm{II}}\big(T, P, \{N_i^{\mathrm{II}}\}\big)$$

$$= \sum_i N_i^{\mathrm{I}} \mu_i^{\mathrm{I}} + \sum_i N_i^{\mathrm{II}} \mu_i^{\mathrm{II}}, \tag{D6}$$

$$= B^{\mathrm{I}}\mu_B^{\mathrm{I}} + B^{\mathrm{II}}\mu_B^{\mathrm{II}} + Q^{\mathrm{I}}\mu_Q^{\mathrm{I}} + Q^{\mathrm{II}}\mu_Q^{\mathrm{II}} + S^{\mathrm{I}}\mu_S^{\mathrm{I}} + S^{\mathrm{II}}\mu_S^{\mathrm{II}}, \tag{D7}$$

where we used Eqs. (16). Interestingly, the total chemical potentials given in Appendix C also fulfill the following equalities:

$$G = B\mu_B + Q\mu_Q + S\mu_S, \tag{D8}$$

$$= G(T, P, B, Q, S). \tag{D9}$$

Note that

$$G^{\mathrm{I}}\big(T, P, \{N_i^{\mathrm{I}}\}\big) = B^{\mathrm{I}}\mu_B^{\mathrm{I}} + S^{\mathrm{I}}\mu_S^{\mathrm{I}} + Q^{\mathrm{I}}\mu_Q^{\mathrm{I}}, \tag{D10}$$

and because we always consider either $S^{\mathrm{I}} = S^{\mathrm{II}} = 0$ or $\mu_S^{\mathrm{I}} = \mu_S^{\mathrm{II}} = 0$, we obtain from Eq. (34)

$$G^{\mathrm{I}} = B^{\mathrm{I}}\mu_B^{\mathrm{I}} + Q^{I}\mu_Q^{\mathrm{I}}, \tag{D11}$$

$$= B^{\mathrm{I}}\tilde{\mu}^{\mathrm{I}}, \tag{D12}$$

so the local $\tilde{\mu}^I$ is also equal to the local Gibbs free energy per baryon.

We remark that the Gibbs free energy per baryon is important because it is just this quantity which must be equal in the case of forced-congruent phase coexistence (under Maxwell conditions), in analogy to the specific Gibbs free energy used for terrestrial chemically reacting plasma.

[1] S. Fiorilla, N. Kaiser, and W. Weise, Nucl. Phys. A **880**, 65 (2012).
[2] V. Somà and P. Bożek, Phys. Rev. C **80**, 025803 (2009).
[3] J. Pochodzalla, T. Möhlenkamp, T. Rubehn, A. Schüttauf, A. Wörner, E. Zude, M. Begemann-Blaich, T. Blaich, H. Emling, A. Ferrero *et al.*, Phys. Rev. Lett. **75**, 1040 (1995).
[4] J. B. Elliott, L. G. Moretto, L. Phair, G. J. Wozniak, L. Beaulieu, H. Breuer, R. G. Korteling, K. Kwiatkowski, T. Lefort, L. Pienkowski *et al.*, Phys. Rev. Lett. **88**, 042701 (2002).
[5] E. Bonnet, D. Mercier, B. Borderie, F. Gulminelli, M. F. Rivet, B. Tamain, R. Bougault, A. Chbihi, R. Dayras, J. D. Frankland *et al.*, Phys. Rev. Lett. **103**, 072701 (2009).
[6] Y.-G. Ma, A. Siwek, J. Péter, F. Gulminelli, R. Dayras, L. Nalpas, B. Tamain, E. Vient, G. Auger, C. O. Bacri *et al.*, Phys. Lett. B **390**, 41 (1997).
[7] Y. G. Ma, J. B. Natowitz, R. Wada, K. Hagel, J. Wang, T. Keutgen, Z. Majka, M. Murray, L. Qin, P. Smith *et al.*, Phys. Rev. C **71**, 054606 (2005).
[8] A. Kurkela, P. Romatschke, A. Vuorinen, and B. Wu, arXiv:1006.4062.
[9] A. Kurkela, P. Romatschke, and A. Vuorinen, Phys. Rev. D **81**, 105021 (2010).
[10] A. Vuorinen, Phys. Rev. D **68**, 054017 (2003).
[11] J. O. Andersen, L. E. Leganger, M. Strickland, and N. Su, Phys. Lett. B **696**, 468 (2011).
[12] J. O. Andersen, L. E. Leganger, M. Strickland, and N. Su, J. High Energ. Phys. 08 (2011) 053.
[13] O. Philipsen, PoS **Confinement8**, 011 (2008).
[14] K. Fukushima and C. Sasaki, arXiv:1301.6377.
[15] D. Blaschke, S. Fredriksson, H. Grigorian, A. M. Öztaş, and F. Sandin, Phys. Rev. D **72**, 065020 (2005).
[16] G. Baym, T. Hatsuda, M. Tachibana, and N. Yamamoto, J. Phys. G **35**, 104021 (2008).
[17] P. D. Powell and G. Baym, Phys. Rev. D **85**, 074003 (2012).
[18] N. Yamamoto, M. Tachibana, T. Hatsuda, and G. Baym, Phys. Rev. D **76**, 074001 (2007).
[19] N. Yamamoto, J. High Energ. Phys. 12 (2008) 060.
[20] H. Abuki, G. Baym, T. Hatsuda, and N. Yamamoto, Phys. Rev. D **81**, 125010 (2010).
[21] J.-L. Kneur, M. B. Pinto, and R. O. Ramos, Phys. Rev. C **81**, 065205 (2010).
[22] J. Steinheimer, V. Dexheimer, M. Bleicher, H. Petersen, S. Schramm, and H. Stocker, Phys. Rev. C **81**, 044913 (2010).
[23] J. Steinheimer, S. Schramm, and H. Stöcker, Phys. Rev. C **84**, 045208 (2011).
[24] O. Lourenco, M. Dutra, A. Delfino, and M. Malheiro, Phys. Rev. D **84**, 125034 (2011).

[25] O. Lourenço, M. Dutra, T. Frederico, A. Delfino, and M. Malheiro, Phys. Rev. D **85**, 097504 (2012).
[26] L. McLerran and R. D. Pisarski, Nucl. Phys. A **796**, 83 (2007).
[27] T. K. Herbst, J. M. Pawlowski, and B.-J. Schaefer, Phys. Lett. B **696**, 58 (2011).
[28] T. Hatsuda, M. Tachibana, N. Yamamoto, and G. Baym, Phys. Rev. Lett. **97**, 122001 (2006).
[29] N. Bratovic, T. Hatsuda, and W. Weise, Phys. Lett. B **719**, 131 (2013).
[30] C. Sasaki and I. Mishustin, Phys. Rev. C **82**, 035204 (2010).
[31] A. Andronic, D. Blaschke, P. Braun-Munzinger, J. Cleymans, K. Fukushima *et al.*, Nucl. Phys. A **837**, 65 (2010).
[32] B. W. Mintz, R. Stiele, R. O. Ramos, and J. Schaffner-Bielich, Phys. Rev. D **87**, 036004 (2013).
[33] M. Di Toro, B. Liu, V. Greco, V. Baran, M. Colonna, and S. Plumari, Phys. Rev. C **83**, 014911 (2011).
[34] M. Di Toro, A. Drago, T. Gaitanos, V. Greco, and A. Lavagno, Nucl. Phys. A **775**, 102 (2006).
[35] G.-H. Zhang and W.-Z. Jiang, Phys. Lett. B **720**, 148 (2013).
[36] G. Y. Shao, M. Di Toro, B. Liu, M. Colonna, V. Greco, Y. X. Liu, and S. Plumari, Phys. Rev. D **83**, 094033 (2011).
[37] B. Liu, M. Di Toro, G. Y. Shao, V. Greco, C. W. Shen *et al.*, Eur. Phys. J. **A47**, 104 (2011).
[38] G. Y. Shao, M. Di Toro, V. Greco, M. Colonna, S. Plumari, B. Liu, and Y. X. Liu, Phys. Rev. D **84**, 034028 (2011).
[39] D. Blaschke, D. E. Alvarez Castillo, S. Benic, G. Contrera, and R. Lastowiecki, arXiv:1302.6275.
[40] G. Baym, H. A. Bethe, and C. J. Pethick, Nucl. Phys. A **175**, 225 (1971).
[41] J. M. Lattimer and D. G. Ravenhall, Astrophys. J. **223**, 314 (1978).
[42] M. Barranco and J. R. Buchler, Phys. Rev. C **22**, 1729 (1980).
[43] H. Müller and B. D. Serot, Phys. Rev. C **52**, 2072 (1995).
[44] C. Ducoin, P. Chomaz, and F. Gulminelli, Nucl. Phys. A **771**, 68 (2006).
[45] A. Lavagno and D. Pigato, Phys. Rev. C **86**, 024917 (2012).
[46] C. Sfienti, P. Adrich, T. Aumann, C. O. Bacri, T. Barczyk, R. Bassini, S. Bianchin, C. Boiano, A. S. Botvina, A. Boudard *et al.*, Phys. Rev. Lett. **102**, 152701 (2009).
[47] A. B. McIntosh, A. Bonasera, P. Cammarata, K. Hagel, L. Heilborn, Z. Kohley, J. Mabiala, L. W. May, P. Marini, A. Raphelt *et al.*, Phys. Lett. B **719**, 337 (2013).
[48] H. Müller, Nucl. Phys. A **618**, 349 (1997).
[49] T. Tatsumi, N. Yasutake, and T. Maruyama, arXiv:1107.0804.
[50] R. Aguirre, Phys. Rev. C **85**, 014318 (2012).
[51] J. B. Clarke, J. W. Hastie, L. H. E. Kihlborg, R. Metselaar, and M. M. Thackeray, Pure Appl. Chem. **66**, 577 (1994).
[52] I. Iosilevskiy, Acta Phys. Polon. B (Proc. Suppl.) **3**, 589 (2010).
[53] L. D. Landau and E. M. Lifshitz, *Statistical Physics, Pt.1* (Pergamon Press, Oxford, and Addison-Wesley, Reading, MA, 1969).
[54] R. C. Reid and T. K. Sherwood, *The Properties of Gases and Liquids* (McGraw-Hill, New York, 1966).
[55] C. Greiner, P. Koch, and H. Stöcker, Phys. Rev. Lett. **58**, 1825 (1987).
[56] N. K. Glendenning, Phys. Rev. D **46**, 1274 (1992).
[57] I. Iosilevskiy, G. J. Hyland, C. Ronchi, and E. Yakub, Int. J. Thermophys. **22**, 1253 (2001).
[58] I. Iosilevskiy, G. Hyland, E. Yakub, and C. Ronchi, Trans. Am. Nucl. Soc. **81**, 122 (1999).
[59] I. Iosilevskiy, V. Gryaznov, E. Yakub, A. Semenov, G. Hyland, and C. Ronchi, in *INTAS-93-66 Final Reports,* European Commission, JRC, Institute for Transuranium Elements, Karlsruhe, 1997, 1999.
[60] C. Ronchi, I. Iosilevskiy, and E. Yakub, *Equation of State of Uranium Dioxide* (Springer, Berlin, 2004).
[61] I. Iosilevskiy, *Non-Ideality and Phase Transitions in Coulomb Systems* (Lambert Academic, Germany, 2011).
[62] I. Iosilevskiy, V. Gryaznov, E. Yakub, C. Ronchi, and V. Fortov, Contrib. Plasma Phys. **43**, 316 (2003).
[63] T. Maruyama and T. Tatsumi, in *American Institute of Physics Conference Series*, edited by S. G. Steadman, G. S. F. Stephans, and F. E. Taylor, Vol. 1441 (American Institute of Physics, 2012) p. 387.
[64] M. Hempel, G. Pagliara, and J. Schaffner-Bielich, Phys. Rev. D **80**, 125014 (2009).
[65] A. N. Sissakian, A. S. Sorin, and V. D. Toneev, arXiv:nucl-th/0608032.
[66] P. Chomaz and F. Gulminelli, Nucl. Phys. A **749**, 3 (2005).
[67] D. G. Ravenhall, C. J. Pethick, and J. R. Wilson, Phys. Rev. Lett. **50**, 2066 (1983).
[68] T. Maruyama, T. Tatsumi, D. N. Voskresensky, T. Tanigawa, and S. Chiba, Phys. Rev. C **72**, 015802 (2005).
[69] W. G. Newton and J. R. Stone, Phys. Rev. C **79**, 055801 (2009).
[70] G. Watanabe and T. Maruyama, arXiv:1109.3511.
[71] S. S. Avancini, C. C. Barros, L. Brito, S. Chiacchiera, D. P. Menezes, and C. Providencia, Phys. Rev. C **85**, 035806 (2012).
[72] X. Na, R. Xu, F. Weber, and R. Negreiros, Phys. Rev. D **86**, 123016 (2012).
[73] M. B. Pinto, V. Koch, and J. Randrup, Phys. Rev. C **86**, 025203 (2012).
[74] H. Heiselberg, C. J. Pethick, and E. F. Staubo, Phys. Rev. Lett. **70**, 1355 (1993).
[75] T. Maruyama, S. Chiba, H.-J. Schulze, and T. Tatsumi, Phys. Lett. B **659**, 192 (2008).
[76] G. Pagliara, M. Hempel, and J. Schaffner-Bielich, J. Phys. G **37**, 094065 (2010).
[77] N. Yasutake, T. Noda, H. Sotani, T. Maruyama, and T. Tatsumi, arXiv:1208.0427.
[78] J. Steinheimer, S. Schramm, and H. Stöcker, J. Phys. G **38**, 035001 (2011).
[79] J. Randrup, Phys. Rev. C **82**, 034902 (2010).
[80] V. A. Dexheimer and S. Schramm, Phys. Rev. C **81**, 045201 (2010).
[81] B. G. Todd-Rutel and J. Piekarewicz, Phys. Rev. Lett. **95**, 122501 (2005).
[82] J. M. Lattimer and Y. Lim, Astrophys. J. **771**, 51 (2013).
[83] J. Piekarewicz, Phys. Rev. C **76**, 064310 (2007).
[84] W. Ebeling, W. Kraeft, and D. Kremp, *Theory of Bound States and Ionization Equilibrium in Plasmas and Solids* (Akademie-Verlag, Berlin, 1976).
[85] H. Shen, H. Toki, K. Oyamatsu, and K. Sumiyoshi, Nucl. Phys. A **637**, 435 (1998).
[86] S. Typel, G. Röpke, T. Klähn, D. Blaschke, and H. H. Wolter, Phys. Rev. C **81**, 015803 (2010).
[87] A. S. Botvina and I. N. Mishustin, Nucl. Phys. A **843**, 98 (2010).
[88] M. Hempel and J. Schaffner-Bielich, Nucl. Phys. A **837**, 210 (2010).

[89] A. R. Raduta and F. Gulminelli, Phys. Rev. C **82**, 065801 (2010).
[90] M. Hempel, T. Fischer, J. Schaffner-Bielich, and M. Liebendörfer, Astrophys. J. **748**, 70 (2012).
[91] N. Buyukcizmeci, A. S. Botvina, I. N. Mishustin, R. Ogul, M. Hempel, J. Schaffner-Bielich, F.-K. Thielemann, S. Furusawa, K. Sumiyoshi, S. Yamada *et al*., Nucl. Phys. A **907**, 13 (2013).
[92] C. Ducoin, K. H. O. Hasnaoui, P. Napolitani, P. Chomaz, and F. Gulminelli, Phys. Rev. C **75**, 065805 (2007).
[93] K. A. Bugaev, M. I. Gorenstein, I. N. Mishustin, and W. Greiner, Phys. Lett. B **498**, 144 (2001).
[94] G. Röpke, M. Schmidt, L. Münchow, and H. Schulz, Nucl. Phys. A **399**, 587 (1983).
[95] P. Papazoglou, D. Zschiesche, S. Schramm, J. Schaffner-Bielich, H. Stocker, and W. Greiner, Phys. Rev. C **59**, 411 (1999).
[96] L. Bonanno and A. Drago, Phys. Rev. C **79**, 045801 (2009).
[97] P. Papazoglou, S. Schramm, J. Schaffner-Bielich, H. Stöcker, and W. Greiner, Phys. Rev. C **57**, 2576 (1998).
[98] J. T. Lenaghan, D. H. Rischke, and J. Schaffner-Bielich, Phys. Rev. D **62**, 085008 (2000).
[99] V. Dexheimer and S. Schramm, Astrophys. J. **683**, 943 (2008).
[100] R. Negreiros, V. A. Dexheimer, and S. Schramm, Phys. Rev. C **82**, 035803 (2010).
[101] V. Dexheimer, R. Negreiros, and S. Schramm, Eur. Phys. J. A **48**, 189 (2012).
[102] K. Fukushima, Phys. Lett. B **591**, 277 (2004).
[103] C. Ratti, M. A. Thaler, and W. Weise, Phys. Rev. D **73**, 014019 (2006).
[104] S. Rößner, C. Ratti, and W. Weise, Phys. Rev. D **75**, 034007 (2007).
[105] K. Fukushima, Phys. Part. Nucl. Lett. **8**, 838 (2011).
[106] Y. Aoki, G. Endrődi, Z. Fodor, S. D. Katz, and K. K. Szabó, Nature **443**, 675 (2006).
[107] Z. Fodor and S. Katz, J. High Energ. Phys. 04 (2004) 050.
[108] I. Iosilevskiy, in *Encyclopedia of Low-Temperature Plasma Physics*, edited by V. Fortov, Vol. I (Nauka, Moscow, 2000), Chap. III.1, pp. 275–292.
[109] K. Nakamura and Particle Data Group, J. Phys. G Nucl. Phys. **37**, 075021 (2010).
[110] E. A. Guggenheim, *Modern Thermodynamics by the Methods of Willard Gibbs* (Methuen & Co., London, 1933).
[111] McGraw-Hil and S. P. Parker, *McGraw-Hill Dictionary of Scientific and Technical Terms* (McGraw-Hill, New York, 2003).
[112] T. Maruyama and T. Tatsumi, J. Phys.: Conf. Ser. **312**, 042015 (2011).
[113] V. E. Fortov, I. T. Iakubov, and A. G. Khrapak, *Physics of Strongly Coupled Plasma* (Oxford University Press, Oxford, 2006).
[114] V. E. Fortov, *Extreme States of Matter: On Earth and in the Cosmos,* The Frontiers Collection (Springer-Verlag, Berlin, 2011).
[115] I. Iosilevskiy and A. Starostin, in *Encyclopedia of Low-Temperature Plasma Physics*, edited by V. Fortov, Vol. I (Nauka, Moscow, 2000) Chap. III.1, pp. 327–339.
[116] L. M. Satarov, M. N. Dmitriev, and I. N. Mishustin, Phys. Atom. Nucl. **72**, 1390 (2009).
[117] J. Randrup, Phys. Atom. Nucl. **75**, 764 (2012).
[118] A. V. Yudin, T. L. Razinkova, and D. K. Nadyozhin, Astron. Lett. **39**, 161 (2013).
[119] I. Iosilevskiy and J. Randrup (unpublished).
[120] T. Fischer, I. Sagert, G. Pagliara, M. Hempel, J. Schaffner-Bielich, T. Rauscher, F.-K. Thielemann, R. Käppeli, G. Martínez-Pinedo, and M. Liebendörfer, Astrophys. J. Suppl. Ser. **194**, 39 (2011).
[121] I. Iosilevskiy and A. Chigvintsev, J. Phys. IV France **10**, 451 (2000).
[122] J.-N. Aqua, S. Banerjee, and M. E. Fisher, Phys. Rev. E **72**, 041501 (2005).
[123] I. N. Mishustin, C. Ebel, and W. Greiner, J. Phys. G Nucl. Phys. **37**, 075201 (2010).
[124] I. Iosilevskiy, in *Encyclopedia of Low-Temperature Plasma*, edited by A. Starostin and I. Iosilevskiy (Fizmatlit, Moscow, 2004), Vol. Suppl. B-III-1, pp. 349–428.
[125] I. Sagert, M. Hempel, G. Pagliara, J. Schaffner-Bielich, T. Fischer, A. Mezzacappa, F.-K. Thielemann, and M. Liebendörfer, Phys. Rev. Lett. **102**, 081101 (2009).
[126] C. P. Singh, P. K. Srivastava, and S. K. Tiwari, Phys. Rev. D **80**, 114508 (2009).
[127] P. K. Srivastava, S. K. Tiwari, and C. P. Singh, Phys. Rev. D **82**, 014023 (2010).
[128] G. Y. Shao, M. Colonna, M. Di Toro, B. Liu, and F. Matera, Phys. Rev. D **85**, 114017 (2012).